Pergamon

Geochimica et Cosmochimica Acta, Vol. 68, No. 22, pp. 4539-4557, 2004

0016-7037/04 $30.00 + .00

doi:10.1016/j.gca.2004.04.020

Mobility of arsenic in a Bangladesh aquifer: Inferences from geochemical profiles, leaching data, and mineralogical characterization

Christopher H. Swartz,[1,*] Nicole Keon Blute,[1,†] Borhan Badruzzman,[2] Ashraf Ali,[2] Daniel Brabander,[1,‡] Jenny Jay,[1,§] James Besancon,[4] Shafiqul Islam,[3] Harold F. Hemond,[1] and Charles F. Harvey[1]

[1]Ralph M. Parsons Laboratory, Civil and Environmental Engineering, MIT, 15 Vassar Street, Cambridge, MA, USA
[2]Dept. of Civil Engineering, Bangladesh University of Engineering and Technology, Dhaka-1000, Bangladesh
[3]Dept. of Civil and Environmental Engineering, University of Cincinnati, Cincinnati, OH, USA
[4]Geosciences Dept., Wellesley College, 106 Central Street, Wellesley, MA, USA

(*Received November* 12, 2002; *accepted in revised form April* 30, 2004)

Abstract—Aquifer geochemistry was characterized at a field site in the Munshiganj district of Bangladesh where the groundwater is severely contaminated by As. Vertical profiles of aqueous and solid phase parameters were measured in a sandy deep aquifer (depth >150 m) below a thick confining clay (119 to 150 m), a sandy upper aquifer (3.5 to 119 m) above this confining layer, and a surficial clay layer (<3.5 m). In the deep aquifer and near the top of the upper aquifer, aqueous As levels are low (<10 μg/L), but aqueous As approaches a maximum of 640 μg/L at a depth of 30 to 40 m and falls to 58 μg/L near the base (107 m) of the upper aquifer. In contrast, solid phase As concentrations are uniformly low, rarely exceeding 2 μg/g in the two sandy aquifers and never exceeding 10 μg/g in the clay layers. Solid phase As is also similarly distributed among a variety of reservoirs in the deep and upper aquifer, including adsorbed As, As coprecipitated in solids leachable by mild acids and reductants, and As incorporated in silicates and other more recalcitrant phases. One notable difference among depths is that sorbed As loads, considered with respect to solid phase Fe extractable with 1 N HCl, 0.2 M oxalic acid, and a 0.5 M Ti(III)-citrate-EDTA solution, appear to be at capacity at depths where aqueous As is highest; this suggests that sorption limitations may, in part, explain the aqueous As depth profile at this site. Competition for sorption sites by silicate, phosphate, and carbonate oxyanions appear to sustain elevated aqueous As levels in the upper aquifer. Furthermore, geochemical profiles are consistent with the hypothesis that past or ongoing reductive dissolution of Fe(III) oxyhydroxides acts synergistically with competitive sorption to maintain elevated dissolved As levels in the upper aquifer. Microprobe data indicate substantial spatial comapping between As and Fe in both the upper and deep aquifer sediments, and microscopic observations reveal ubiquitous Fe coatings on most solid phases, including quartz, feldspars, and aluminosilicates. Extraction results and XRD analysis of density/magnetic separates suggest that these coatings may comprise predominantly Fe(II) and mixed valence Fe solids, although the presence of Fe(III) oxyhydroxides can not be ruled out. These data suggest As release may continue to be linked to dissolution processes targeting Fe, or Fe-rich, phases in these aquifers.

1. INTRODUCTION

Arsenic contamination in the groundwaters of Bangladesh is widespread and poses a significant health risk to the millions who depend on this water (Chowdhury et al., 2000; Karim et al., 2000). Beginning in the 1960s, shallow (10–75 m) wells, or tubewells, were drilled throughout Bangladesh to provide drinking water. Surface water consumption had been a primary source of waterborne disease in Bangladesh, and groundwater was thought to be a safe alternative. Unfortunately, much of the water extracted from the alluvial aquifers contains naturally occurring As from the alluvium deposited on the Ganges, Brahmaputra, and Megna river floodplains during the Holocene (BGS & DPHE, 2001). The high concentrations of As in well water came to public attention in 1993, when the Bangladesh Department of Public Health Engineering tested wells in western Bangladesh after extensive As contamination was discovered in West Bengal nearly a decade before (Chadha and Ray, 1999; BGS & DPHE, 2001). Since then, high levels of As have also been found in northwestern Bangladesh (Badruzzaman et al., 1998) and in many of the wells in central and southern Bangladesh (BGS & DPHE, 2001). In a national survey of 3534 wells less than 150 m deep, As concentrations exceeded the Bangladesh standard of 50 μg/L in 27% of the wells, and As concentrations greater than 1000 μg/L were found in some (BGS & DPHE, 2001). It is unclear what proportion of the population (>120 million) will eventually suffer health effects as a result of exposure (Anawar et al., 2002), but the implication of existing dose-response data (Mazumder et al., 1998) is that the prevalence of arsenocosis will be more than one million people (Yu et al., 2003).

Observations of low oxidation/reduction potential, high levels of aqueous Fe and bicarbonate, and low levels of sulfate, have led researchers to hypothesize that microbially mediated reduction of Fe(III) oxyhydroxides has been the primary mechanism mobilizing As from these shallow sediments (Bhatta-

* Author to whom correspondence should be addressed, at Stockholm Environment Institute/Tellus Institute, 11 Arlington Street, Boston, MA 02116, USA (cswartz@tellus.org).
† *Present address:* McGuire Environmental Consultants, 119 Santa Monica Blvd., Suite 200, Santa Monica, CA, USA.
‡ *Present address:* Wellesley College, Wellesley, MA, USA.
§ *Present address:* Dept. of Civil and Environmental Engineering, University of California, Los Angeles, CA, USA.

charya et al., 1997; Nickson et al., 1998, 2000; BGS & DPHE, 2001; Harvey et al., 2002). Although release of As through oxidation of pyrite has also been advanced as a mobilization mechanism (Chowdhury et al., 1999), regional (Nickson et al., 2000; BGS & DPHE, 2001) and local geochemical surveys (Harvey et al., 2002) indicate an inverse relationship typically exists between dissolved sulfate and As in the pore waters of the Holocene aquifers, inconsistent with patterns expected from dissolution of arsenical pyrite. In addition, acid volatile sulfides have been detected in sediments cored throughout the depth range of peak aqueous As concentrations at one site within a highly impacted area south of Dhaka (Harvey et al., 2002), suggesting that formation, rather than oxidative dissolution, of sulfides is more likely in these deposits.

While country-wide surveys have mapped the extent of dissolved As contamination in tubewells, only a few studies have been devoted to the analysis and characterization of the sediments to elucidate what role solid phases play in As mobility in these aquifers (Foster et al., 2000; Nickson et al., 2000; BGS & DPHE, 2001; Breit et al., 2001). Nickson et al. (2000) extracted "diagenetically available" metals from late Pleistocene-Holocene sediments taken from two shallow cores collected from the Gopalganj district using hot concentrated HCl and found Fe and As in these extracts to be correlated. BGS & DPHE (2001) analyzed sediments taken from up to 150 m in depth in several districts of Bangladesh. In addition to mineralogical characterization by scanning electron microscopy and X-ray diffraction, they used selective dissolution with ammonium oxalate to liberate solid phase As. They found ammonium oxalate-extractable As and Fe to be highly correlated. Extraction methods used by Nickson et al. (2000) and BGS & DPHE (2001) did not differentiate sorbed versus coprecipitated As. Breit et al. (2001) and Foster et al. (2000) analyzed shallow (<50 m) sediments using X-ray absorption spectroscopy, finding evidence for As associated with aluminum hydroxides and the weathered, Fe-rich edges of phyllosilicates in gray, reduced sediments of the Holocene aquifer.

Data characterizing deeper aquifer materials are particularly sparse, and little work has been done with the orange-brown Pleistocene sediments typically underlying a confining clay layer present at up to 50 m in thickness in some areas of Bangladesh. The pore water extracted from wells deeper than 150 m typically has much lower As concentrations (van Geen et al., 2003a), with only 5% of wells sampled in the national survey exceeding 10 ug/L (BGS & DPHE, 2001). For this reason, deeper wells, some penetrating the Pleistocene sediments below the confining clay layer, are currently being installed in some villages as a presumably safe alternative to the As-contaminated shallower wells (van Geen et al., 2003b; Yu et al., 2003). These installation programs are in addition to the deep well installations that have occurred in past years in the coastal areas to remedy saline intrusion. However, it is not known whether these deeper wells will remain free of As once extraction of water from the wells commences. Deeper wells, especially those completed where a confining unit is absent, might become contaminated with time if As moves downward from the shallower aquifer, induced by deep well pumping (BGS & DPHE, 2001). Shifts in geochemical conditions resulting from pumping may also facilitate As mobilization to pore water. To our knowledge, no analyses of the deeper aquifer below this clay confining layer have been conducted to determine at what concentrations, and in what forms, As is present in these sediments. These issues need to be addressed before future water use from the deeper aquifer can be planned.

The objectives of the present study are therefore to contribute to understanding the geochemical mechanisms that control partitioning of naturally occurring As between aquifer solids and groundwater in the aquifers of Bangladesh. We provide a detailed geochemical characterization of aqueous and solid phases along a depth profile extending to 165 m below ground surface at a site in a village within the Munshiganj district south of Dhaka, Bangladesh. Our investigation also includes one of the first analyses of sediments taken from the deeper aquifer underlying the clay aquiclude. These data complement an earlier presentation of aqueous and solid phase profiles from this site by Harvey et al. (2002), who showed that aqueous Ca and NH_4^+ closely follow the profile of aqueous As throughout the upper aquifer, which peaks at a depth range of 30 to 40 m, and aqueous inorganic carbon and organic carbon (DOC) also increase with increasing As up to the peak depth. They inferred from these observations that microbial respiration and associated ammonification of organic matter resulted in the reductive dissolution of Fe(III) oxyhydroxides and possibly dissolution of calcite as well, the former being a likely cause of the elevated aqueous As levels in the upper aquifer (Harvey et al., 2002). Furthermore, they demonstrated the susceptibility of upper aquifer sediments to further release of As to pore water after introduction of labile organic matter to stimulate microbial respiration (Harvey et al., 2002), suggesting that some As may yet be associated with solid phases susceptible to reductive dissolution.

In this paper, we provide additional analyses of dissolved constituents from this site as well as characterization of solid phase As. We use sequential extraction techniques to differentiate between adsorbed and coprecipitated As in the sediments and to quantify readily extractable Fe versus Fe incorporated in more recalcitrant phases such as silicate minerals and pyrite. Although the utility of extraction methods can be limited by nonselectivity (Ryan and Gschwend, 1991) and readsorption of target elements (Gruebel et al., 1988; Ostergren et al., 1999), their application can aid in characterizing relative leachability of elements from sediment matrices. We also use spectroscopic methods to elucidate spatial associations between As and Fe in sediment matrices. In addition, we perform geochemical equilibrium modeling, with input parameters provided from the aqueous and solid phase analyses, to explore whether amorphous Fe(III) oxyhydroxide, even as only a relatively small amount of the total pool of readily extractable Fe, could explain dissolved and solid phase levels of As in the upper aquifer, as suggested by the in-situ mobilization experiments conducted by Harvey et al. (2002). We use a depth where aqueous As is highest as an example for this exercise. With the intent to inform more reliable evaluation of alternative water supply options for Bangladesh, these analytical methods are used in an effort to understand the mobility of As in sediments in the upper and lower aquifers and, in particular, what types of geochemical alterations, possibly induced by pumping, may further mobilize any As present in these aquifers.

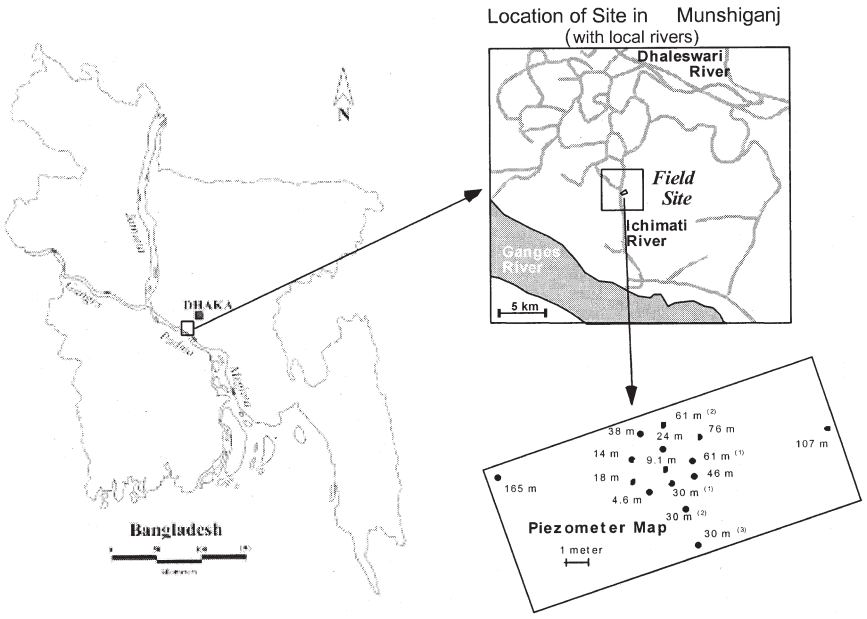

Fig. 1. Map showing the approximate location of the study site with regard to Dhaka and within the Munshiganj district (first inset). The second inset shows the relative positions of the 15 monitoring wells (circles). Fourteen monitoring wells were penetrated in the shallow aquifer with well screens ending at 4.6, 9.1, 14, 18, 24, 30, 38, 46, 61, 76, and 107 m in the shallow aquifer, and one well was placed in the deeper aquifer with a screen ending at 165 m. Three 30-m and two 61-m monitoring wells were installed. See text for well screen lengths.

2. FIELD SITE AND METHODS

2.1. Site Location

This work was carried out in the village of Bejgaon, near the village of Sreenagar in the Munshiganj district of Bangladesh, approximately 20 km south of Dhaka and 6 km north of the Padma (Ganges) (Fig. 1). The upper aquifer underlying the Munshiganj district is of similar lithology as the heavily As-contaminated aquifers within the Faridpur, Chandpur, and Gopalganj districts south of the Ganges River. Up to 83% of the analyzed tubewells in the Munshiganj district have been found to contain greater than 50 μg/L As (BGS & DPHE, 2001).

Reconnaissance of 18 shallow (30 to 61 m) drinking water wells within two kilometers of the site showed As concentrations (measured by GFAA, see below) ranging between 100 μg/L to 1040 μg/L with an average of 290 $\pm$ 220 μg/L. The maximum concentration was recorded at a well located 50 m from the selected site. Waters from these wells were characterized by dissolved Fe(II) levels ranging between 4.5 to 8.4 mg/L, Mn(II) levels between 0.05 to 0.96 mg/L, chloride levels between 10 to 200 mg/L, silicate levels between 40 to 70 mg/L as SiO_2, and nitrate levels between $<$0.1 to 0.25 mg/L as NO_3-N.

2.2. Sample Collection

2.2.1. Sediment collection

A rotary drill rig and a split-tube sampler accepting 50 mm O.D. PVC liner were used to extract sediment cores in 61 cm long increments down to a depth of approximately 150 m in April, 2000. Coring was continuous to a depth of 61 m, every 1.5 m to 91 m, and every 3 m to approximately 120 m, with recovery estimated to be 75% or greater to this depth. Sediment sample collection from the clay layer (120 to 150 m) was limited to 122 m and 125 m due to poor core recovery with the split-tube, and borehole collapse prevented collection of sediments from this hole below the base of the clay layer (150 m). Sediment samples from four depths below the clay layer (155 m, 159 m, 162 m and 165 m) were obtained during manual drilling of a 165 m monitoring well (see section 2.2.2). Additional 61 cm long cores were collected continuously using the rotary drill rig from the depth range of 25 to 31 m in January 2002. These cores were collected to provide fresh sediment with which to analyze further the chemical nature of the solid phase, particularly the oxidation state of Fe.

To limit contact of cored sediment with the atmosphere, the split tube sampler was opened upon retrieval, and melted paraffin wax was poured into the open ends of the PVC liner. The sealed cores were taken back to the Bangladesh University of Engineering and Technology (BUET) lab in Dhaka, where cores were subsampled and archived within 24 h. All manipulation of core materials was conducted in a polyethylene glove-bag purged with N_2, and no visible signs of oxidation were observed at the edges of cored material when the cores were later opened and subsampled. To exclude from subsequent analyses sediment that may have come in contact with drilling fluids, only sediment from the middle of each 61 cm-long core was subsampled. Each of the cores was cut in half, and approximately 100 g of sediment was spooned out of each of the freshly cut ends of the liner from the middle of the core, using a Teflon spatula, into a high density polyethylene (HDPE) bottle. Depths to the middle of the 61 cm core lengths were recorded for these samples. Sample bottles were placed in secondary HDPE containers and frozen before shipment to MIT. Thawing of samples did occur during the roughly 48 h in transit, but were stored refrozen until needed. Sediment aliquots from the middle of cores were also archived for acid volatile sulfide (AVS) analysis (refer to section 2.3.2 below), which was conducted within 48 h of core collection at BUET. Note that, although the loose samples collected for the four depths in the lower aquifer were immediately bagged and frozen for preservation, brief contact with atmosphere and oxygenated water did occur due to the nature of the drilling process.

2.2.2. Monitoring well construction

Groundwater was sampled from an array of 15 monitoring wells (Fig. 1, inset) screened at discrete depths down to 165 m. A manual drilling technique practiced in rural Bangladesh (the "sludger" method; BGS & DPHE, 2001) was used to construct the 50 mm O.D. PVC monitoring wells at depths of 4.6 m, 9.1 m, 14 m, 18 m, 24 m, 30 m (3 each), 38 m, 46 m, 61 m (2 each), 76 m, 107 m, and 165 m. This percussion-based method involved systematically and repeatedly lifting and dropping, via a lever attached to a bamboo derrick, a 6.1 m length of 7.5 cm O.D. steel casing attached to 5 cm O.D. PVC pipe (referred

to below as the percussion tool). The deepening hole was flushed with water to create a slurry at its base. As the casing was lifted, an operator positioned at the top of the derrick placed his hand over the open end of the percussion tool to create suction. As the percussion tool was dropped down the hole, the operator raised his hand from the end of the percussion tool, allowing the slurry at the base of the hole to be driven up and out through the pipe. As the hole deepened, more PVC pipe extensions were added to the percussion tool.

When the desired depth was reached, the percussion tool was lifted out of the hole and the permanent well screen and casing, constructed of 3 m lengths of 50 mm O.D. PVC, were lowered down the hole. The well screen lengths for wells shallower than 30 m, between 30 and 107 m in depth, and the 165 m deep well were 1.5 m, 3 m, and 6.1 m long, respectively. The PVC pipes for each well were joined by first softening one end with a flame, then inserting another pipe to create a seamless joint that would easily slide down the well bore. Sand was poured down the annulus between the casing and the hole to backfill the screened interval. The sand was followed with quick-setting cement, which was used to fill the annulus up to ground surface to prevent short-circuiting of flow between various depths.

2.2.3. Water sampling

Wells were sampled by peristaltic pump (Cole Parmer) with 6 mm O.D. HDPE tubing lowered to the depth of the middle of the well screen. Inflatable packers were used to isolate the screened interval in all wells shallower than 46 m. Because of pressure limitations for the packers, deeper wells were pumped without packers installed. However, no drawdown of the water level in the wells (approximately 2 m below ground surface) was observed during pumping, indicating that pumped water was drawn from the aquifer and not the well bore. Before sampling, all wells were pumped at a flow rate of 6 L/min for at least 1 h to allow the discharge to clarify (turbidity was not measured) and to develop the wells.

Samples were collected at a flow rate of approximately 200 mL/min and water quality measurements were made in a manner to exclude contact with the atmosphere. A multi-probe flow cell (Geotech Environmental Equipment, Denver, CO) fitted with calibrated pH, platinum redox, conductivity, and dissolved oxygen electrodes was placed in the sampling line. Electrode parameters were recorded after readings stabilized (e.g., remained unchanged for at least 4 L of discharge).

A 147 mm diameter polycarbonate filter cartridge (Geotech Environmental Equipment, Denver, CO) containing a 200 nm polycarbonate filter membrane (Osmotics) was then placed in the sample line. Downstream of this cartridge, a 125 mL HDPE bottle was also added to the sample line. Two 3-way stopcocks fitted to the bottle lid allowed exchange of the bottle, once filled, without contact with the atmosphere. Downstream of this collection point was another 147 mm diameter polycarbonate filter cartridge containing a 50 nm polycarbonate filter membrane, followed by another sampling point. We collected several 125 mL volumes of 200 nm and 50 nm filtrate. Immediately following collection, both 200 nm and 50 nm filtered samples were placed in a N_2-purged polyethylene glove-bag at the field site, and sample aliquots were separated out either for analysis on-site or archived for future laboratory analyses (see section 2.3.1). Samples of unfiltered water were also collected for total metals and dissolved organic carbon analyses.

2.3. Analytical Methods

2.3.1. Aqueous analyses

2.3.1.1. Field. Aliquots of the 200 nm filtrate were analyzed immediately on-site using Chemets (Chemetrics, VA) for the following dissolved constituents: Fe(II), total Fe, Mn(II), total sulfide, NH_4^+-N, NO_3^--N, and total phosphate. These measurements were conducted initially in a glove-bag filled with N_2, but replication of sample analyses outside of the glove-bag showed identical results to those conducted inside the glove-bag. All subsequent Chemets analyses were conducted outside the glove-bag. Additional aliquots of 200 nm filtrate were saved for ion chromatography and measurement of alkalinity, total metals and dissolved CO_2 (by filling a gas-tight syringe with sample) at MIT.

Aliquots of the 50 nm filtrate from each well depth were immediately subjected to a technique to separate the As(III) (arsenite) and As(V) (arsenate) species (Edwards et al., 1998). These separations were conducted in the glove-bag and performed in duplicate for each well depth except 4.6 m. 50 mL aliquots of sample were passed through a cartridge containing approximately 2 g of moist Biorad resin, which traps the As(V) species, at a flow rate of approximately 5 mL/min. Samples were not first acidified to pH 2.5–3.0 with sulfuric acid as specified by Edwards et al. (1998) due to lack of ultra-pure reagent. Failure to acidify samples before separation may result in underestimation of the fraction As(III) due to trapping of a portion of As(III) onto the resin (Edwards et al., 1998), particularly at the ambient circumneutral pH of our samples. Recovery experiments were performed later with standard solutions to estimate the extent of As(III) underestimation due to not acidifying samples (see section 3.2.2). Effluent from the columns was collected for analysis of As (assumed As(III) species) content. The resin was then emptied out of the cartridge into a 50 mL centrifuge tube, to which 10 mL of 1 mol/L HCl was added to elute As trapped on the resin. The tube was shaken for 5 min, the resin allowed to settle, and aliquots of the supernatant were sampled for later analysis of As (assumed As(V) species) content.

2.3.1.2. Laboratory. All measurements were performed at MIT unless noted otherwise. Concentrations of As in the Biorad resin filtrate and eluent, the unfiltered samples, and the 200 nm and 50 nm filtrates were measured by graphite furnace atomic absorption spectrophotometry (GFAA) (Perkin Elmer, 4100ZL) with a detection limit of 5 μg/L or by hydride generation-fluorescence spectrophotometry (HGFS) (PSA Excalibur) with a detection limit of 150 ng/L. Matrix modifiers used in the GFAA analyses comprised 250 mg/L palladium (as palladium chloride) and 150 mg/L magnesium nitrate. The 200 nm filtrates were also analyzed for aluminum and silicon (by GFAA), molybdate-reactive silica (Standard Methods for the Examination of Water and Wastewater, 1992), the major cations Na, K, Ca, and Mg (by flame atomic absorption spectrophotometry, Perkin Elmer AAnalyst100), and chloride and sulfate (by ion chromatography, Dionex model 16 with a self-regenerating anion suppressor column). Bicarbonate was calculated from alkalinity, measured in the 200 nm fitrates by Gran titration to pH 3 with 1 mM HCl, after correcting for other measured contributors to alkalinity. Dissolved CO_2 was measured by GC analysis (Hewlett Packard fitted with a CarboSieve column) of a N_2 headspace equilibrated with 200 nm filtrate in a 50 mL gas-tight syringe preserved in the field. Nonpurgeable dissolved organic carbon was measured in unfiltered samples, after acidification to pH 3 and purging with N_2, by combustion and infrared detection of CO_2 (TOC-5000, Shimadzu) standardized with potassium hydrogen phthalate.

2.3.2. Sediment analyses

2.3.2.1. Bulk chemical analysis. Aliquots of sediment from the archived core samples were analyzed for a variety of elements, including As, Fe, and S using polarized energy dispersive X-ray fluorescence (EDXRF) with an X-Lab2000 (Spectro Analytical) and Turboquant data analysis routines (for methodologic details, see Rogers et al., 2002). Solid phase C was determined with a model 2400 CHN analyzer (Perkin Elmer).

2.3.2.2. Extractions. Extractions to indicate the presence of acid volatile sulfide (AVS) in the sediment samples were performed at the BUET lab within 48 h after recovery of the cores. 40 mL of 1 mol/L HCl was added to each previously archived 2.5 g moist sediment sample in 50 mL centrifuge tubes (see section 2.2.1). The suspension was purged by bubbling with N_2 at approximately 40 mL/min, and the gas was carried via Teflon tubing to 250 mL Sepcor bottles containing 0.3 mol/L zinc acetate and 0.12 mol/L sodium acetate to trap hydrogen sulfide as zinc sulfide. Sulfide was measured spectrophotometrically using the methylene blue method (Hach DR 4000U UV Spectrophotometer).

Sequential extraction (Keon et al., 2001) was performed at MIT to differentiate pools of solid phase As within 1 yr of sample collection. This method targets weakly adsorbed As (1 mol/L $MgCl_2$, pH 8), strongly adsorbed As (1 mol/L NaH_2PO_4, pH 4–5), As coprecipitated

with carbonates, acid volatile sulfides, amorphous metal oxides and magnetite (1 mol/L HCl followed by 0.2 mol/L oxalic acid, pH 3), As coprecipitated with crystalline Fe oxides and amorphous sulfides (0.5 mol/L titanium(III)chloride-sodium citrate-tetrasodium EDTA-bicarbonate, pH 7), As coprecipitated with silicate minerals or As_2O_3 (10 mol/L hydrofluoric acid), and As incorporated in pyritic phases (concentrated nitric acid). A final hot concentrated nitric acid and hydrogen peroxide digest (EPA method 3050B) of the residue targets As incorporated in crystalline sulfides such as orpiment, and other recalcitrant phases (Keon et al., 2001). These extraction steps are referred to hereafter as MG, PHOS, HCl, OX, TiCEB, HF, NIT, and HOT NIT, respectively.

Sediment samples were thawed, then manipulated in a glove-box purged with N_2. All extractant solutions were made up in deoxygenated 18 MOhm water (with less than 1 μM O_2, as measured by Chemets). Thirty mL of each extractant was added to 2.5 g of moist sediment in a 50 mL Sepcor centrifuge tube. Suspensions were shaken for the prescribed amount of time, centrifuged at 23,000 *g* for 30 min, and the supernatant decanted. The next extractant was added and the procedure was repeated. Levels of As in the extracts were measured by either GFAA or HGFS, with standards prepared in the appropriate matrices. Fe liberated in each of the extraction steps was measured by GFAA.

Aliquots of the HCl extracts were also analyzed with the ferrozine method (Gibbs, 1979; Lovley and Phillips, 1986) to determine the amount of liberated Fe(II), and after reduction via addition of hydroxylamine hydrochloride (Gibbs, 1979), total Fe. These latter analyses were performed mostly on core samples obtained in January 2002, within 8 weeks of sample collection. Samples from a few matching depths from the older core (April 2000) were concurrently analyzed to determine whether oxidation of this material had occurred in storage since collection (approximately 2 yr). No attempt was made to speciate Fe liberated by the OX extractant due to the difficulty in preserving the oxidation state of Fe in this extractant. Oxalate degrades rapidly in light and promotes reduction of Fe(III) (Cornell and Schindler, 1987; Panias et al., 1996).

A separate one-step extraction was performed on aliquots from the same sample depths to quantify adsorbed phosphate and silicate; phosphate could not be quantified in the PHOS leaches due to interference from the extractant. 2.5 g of moist sediment was placed in a centrifuge tube and 30 mL of deoxygenated water, acidified to pH 2.0 with HCl, was added. The suspension was shaken for 4 h, centrifuged, and decanted. Phosphate was measured by the stannous chloride-molybdate method (Standard Methods for the Examination of Water and Wastewater, 1992) and silicate was inferred from GFAA analysis for silicon. As liberated by the pH 2 extractant was quantified by HGFS for comparison with levels determined from the MG and PHOS leaches performed in the parallel sequential extraction procedure.

2.3.2.3. Density and magnetic separations. Density separations were conducted on air-dried samples from four depths (9.6, 27.7, 74.7, and 165 m) to quantify As associations as a function of density class. Bromoform (Geoliquids, Inc.) was used to separate grains with densities greater than and less than 2.85 g/cm^3. The >2.85 g/cm^3 fraction was separated by running a hand magnet over the samples, and the hand-magnetic fraction was collected. The portion of the sample not collected by the hand magnet was further separated with a Franz isomagnetic analyzer into 0.5 and 1.5 amp fractions. The remainder was classified as nonmagnetic. Cumulative recoveries for the density and magnetic separations were always greater than 85%.

2.3.2.4. NAA, XRD, SEM and X-ray microprobe analyses. Sediment fractions separated by density and magnetic properties were placed in the 5.0 MW M.I.T research reactor and subjected to thermal neutron flux of 8×10^{12} n/cm^2/s. Irradiations lasted between 30 s to 6 h depending on the half-life of the elements of interest. Germanium-based gamma ray detectors coupled with the Genie 2000 neutron activation analysis program were used to calculate the concentration of trace elements with ng/gm detection limits for many of the elements of interest. The standardization process used two NIST standards, one run as a sample with every batch of samples, i.e., every 6 to 10 samples.

Aliquots of the density and magnetic separates were also hand ground and mounted on glass slides as slurry. X-ray diffraction measurements used CuKα radiation and a graphite monochrometer on a Philips vertical diffractometer, stepped at 6 s/0.02°, from 4° to 100° 2θ. Iterative identification of minerals in the samples used Jade software (Materials Data Incorporated) with Search/Match of the FIZ/ICSD minerals database using calculated powder patterns, and Rietveld whole pattern fitting options. Initial full physics model refinements of obvious major phase(s) left a residual pattern that was iteratively rematched with the database and refined until no additional likely phases resulted. Atom coordinates including occupancies were not refined as the complexity of the mixtures together with pattern quality did not justify these steps. The final refinement gave unit cell and approximate abundance of each mineral (based on the formula of the database match and calculated density and not taking into account possible microabsorption), normalized to 100%. This procedure does not include possible undiscovered minor phases or amorphous fractions.

Observation and characterization of elemental composition of mineral grains was conducted with scanning electron microscopy (SEM) and energy dispersive spectroscopy (EDS) using a variable pressure LEO-433VP instrument (LEO Instruments). Quantitative analysis was performed with an IXRF 10 mm^2 active over Si (Li) detector.

X-ray microprobe analyses were also conducted to elucidate spatial associations between As and Fe in sediment samples. Sediment aliquots from depths of 29.5 m and 165 m were analyzed by X-ray microprobe at undulator beamline 13-ID-C of the Advanced Photon Source (APS), Argonne National Laboratory. Samples used in this analysis were parafilm-sealed and stored frozen at −30°C during the 9 month period between arrival at MIT and beamtime availability. In a N_2-purged glove-box at the APS, an aliquot from the center of each bottle was removed with a Teflon spatula, and a thin layer of sediment was applied to a piece of 8 μm thick Kapton tape attached to a cardboard slide mount. Fluorescence data for As and Fe were collected using a solid-state, energy-dispersive, multi-channel Ge detector. A 5 μm step size was used for elemental mapping of 400 × 340 μm scan areas. Because of low As concentrations in the samples and a temporarily compromised detector, we were only able to map elemental distributions but not collect adequate absorption spectra to determine solid phase As speciation and binding mechanisms.

2.3.2.5. Aqueous and adsorption modeling. MINEQL (version 4.0+) was used to test hypothesized mechanisms of As sorption in the upper aquifer. The modeled sorbent was amorphous Fe(III) oxyhydroxide, and the Two Layer Model (TLM) for hydrous ferric oxide (HFO) within MINEQL was used. The central component of the TLM is the Diffuse Layer Model (DLM) (Dzombak and Morel, 1990). Ligand sorption was considered to occur at a single surface site type, with a density of 0.2 mol/mol Fe (Dzombak and Morel, 1990). Equilibrium sorption constants for arsenite, arsenate, and phosphate species on HFO were used from the MINEQL thermodynamic database (Table 1). Equilibrium constants needed to model three sorbed silicate species, $\equiv FeH_3SiO_4^0$, $\equiv FeH_2SiO_4^-$, and $\equiv FeHSiO_4^{2-}$, on HFO were taken as the weighted average intrinsic adsorption constants from Swedlund and Webster (1999) (Table 1). Equilibrium constants describing adsorption of two carbonate species ($\equiv FeOCO_2^-$, and $\equiv FeOCO_2H$) onto HFO were taken from Appelo et al. (2002). Carbonate ion concentrations were calculated from alkalinity and pH.

Total As concentrations for the one well depth (30 m) used in simulations were derived by adding the measured dissolved As concentration to the averaged sum (from at least two depths within the well screen depth interval being considered) of adsorbed As leached by the pH 2 extractants, corrected to aqueous molar quantities using an assumed porosity of 0.30 and a solids density of 2.6 g/cm^3 (Table 1). Total phosphate and silicate concentrations were calculated similarly (Table 1). Total Fe(III) concentrations (allowed to precipitate as HFO in the simulations) were derived by assuming that a fraction of Fe leached by the OX extractant was liberated from amorphous Fe(III) oxyhydroxides (with surface properties identical to HFO). The quantity of Fe liberated by the HCl extracts was added to aqueous Fe(II) to determine total Fe(II) for these simulations. In additional simulations, amorphous silica (GL), siderite [$FeCO_3$], and vivianite [$Fe_3(PO4)_2$] were also allowed to precipitate.

Because the speciation of As in the pH 2 extractant was not deter-

Table 1. Parameters used in MINEQL modeling of the 30 m well depth.

Adsorption reaction	log K^{int}
$\equiv FeOH + H^+ \leftrightarrow FeOH_2^+$	7.29
$\equiv FeOH \leftrightarrow \equiv FeO^- + H^+$	−8.93
$\equiv FeOH + AsO_3^{3-} + 3H^+ \leftrightarrow \equiv FeH_2AsO_3 + H_2O$	40.20
$\equiv FeOH + PO_4^{3-} + 3H^+ \leftrightarrow \equiv FeH_2PO_4 + H_2O$	31.29
$\equiv FeOH + PO_4^{3-} + 2H^+ \leftrightarrow \equiv FeHPO_4^- + H_2O$	25.39
$\equiv FeOH + PO_4^{3-} + H^+ \leftrightarrow \equiv FePO_4^{2-} + H_2O$	17.72
$\equiv FeOH + H_4SiO_4 \leftrightarrow \equiv FeH_3SiO_4 + H_2O$	4.28[a]
$\equiv FeOH + H_4SiO_4 \leftrightarrow \equiv FeH_2SiO_4^- + H^+ + H_2O$	−3.22[a]
$\equiv FeOH + H_4SiO_4 \leftrightarrow \equiv FeHSiO_4^{2-} + 2H^+ + H_2O$	−11.69[a]
$\equiv FeOH + CO_3^{2-} + H^+ \leftrightarrow \equiv FeOCO_2^- + H_2O$	12.78[b]
$\equiv FeOH + CO_3^{2-} + 2H^+ \leftrightarrow \equiv FeOCO_2H + H_2O$	20.37[b]

Total concentrations for 30 m depth				
As (mg/L)[c]	PO_4 (g/L)[d]	$Si(OH)_4$ (g/L as Si)[d]	Fe^{3+} (g/L)[e]	Fe^{2+} (g/L)[g]
2.58 (0.51, 2.07)	1.46 (0.004,1.46)	1.03 (0.02,1.01)	7.65 (nd[f],7.65)	16.6 (0.01,16.6)

[a] Taken from Swedlund and Webster (1999).
[b] Taken from Appelo et al. (2002).
[c] The sum of [dissolved As measured in well] + [sum of pH 2-extractable As averaged for at least two sample depths within the well screen depth range]. The numbers in parentheses are the respective values for each of these two bracketed components.
[d] The sum of [dissolved phosphate or silicate measured in well] + [sum of pH 2-extractable phosphate or silicate averaged for at least two sample depths within the well screen depth range]. The numbers in parentheses are the respective values for each of these two bracketed components.
[e] The sum of OX-extractable Fe averaged for at least two sample depths within the well screen;
[f] nd = dissolved Fe(III) was not detected; total dissolved Fe was indifferentiable from dissolved Fe(II).
[g] The sum of [dissolved Fe(II) measured in well] + [HCl-extractable Fe averaged for at least two sample depths within the well screen]. The numbers in parentheses are the respective values for these two bracketed components.

mined, initial simulations were run for the 30 m depth (Table 1) to ascertain whether the model would predict dominance of arsenate or arsenite in the adsorbed As pool. Total As, phosphate, silicate, carbonate, Fe(II), and Fe(III) (all in Table 1), as well as pH and major ion concentrations (Table 2), were held constant while the percentage of As(III) was varied from a lower bound of 20% of total As (obtained if arsenite existed only in the aqueous phase, and not in the adsorbed pool, at 30 m; see Table 1) to 90%. Only HFO was allowed to precipitate, and OX-extractable Fe was taken as total Fe(III) in these simulations.

3. RESULTS

3.1. Lithology

The site is overlain by a 3.5 m thick gray clay layer unsaturated to a depth of approximately 2 m, the maximum drawdown of the water table during dry season irrigation, at the time of sediment collection (Fig. 2a). Below this layer, intercalated fine sands and silty sands, gray in color, were observed to a depth of approximately 12 m. A sequence of fine to medium sands, grayish-green in color, was collected from 12 to 110 m, interrupted by a 10 cm thick silty-clay layer observed at 42.5 m and a silty-fine sand layer, approximately 1.5 m thick, at 76 m. Intercalated fine sands and silty clays were observed from 110 m to 119 m, below which a greenish clay was encountered to a depth of 150 m (Fig. 2a). Fine to medium sands were encountered at depths from 150 to 165 m. These sands were light brown to orange in color, contrasting with the grayish-green sands in the upper aquifer. For this study, the sediments located above the 30 m thick clay layer will be referred to as the "upper" aquifer and are presumed to be Holocene deposits. Sediments beneath the clay layer will be referred to as the "lower" aquifer and are presumably Pleistocene.

3.2. Geochemical Profiles and Redox Conditions

3.2.1. General chemistry

Values for aqueous parameters measured in individual wells are presented in Table 2. pH ranges from 6.6 (4.6 m) to 7.1 (107 m) in the upper aquifer, and a value of 6.8 was measured in the one well in the lower aquifer (165 m) (Fig. 2b). Aqueous constituents are dominated by HCO_3^-, Ca, Mg, and Na in the upper aquifer and by Cl^- and Na in the lower aquifer (Figs. 2c,d). Conductivity generally increases with depth, from 530 μS/cm at 4.6 m in the upper aquifer to 1900 μS/cm at 165 m in the lower aquifer (Table 2).

3.2.2. As distribution

Unfiltered aqueous As concentrations exhibited strong depth dependence, increasing from 6 ± 1 μg/L (error is one standard deviation of two replicate analyses) at both the 4.6 m and 9.1 m depths to 640 ± 19 μg/L at one 30 m well (30-1) (Fig. 3a). Aqueous As concentrations of 490 ± 4 μg/L and 390 ± 1 μg/L in the two other wells screened at 30 m (30-2 and 30-3) and located only 3 m and 6.1 m distant (Fig. 1, inset) from well 30-1 demonstrate lateral variability in aqueous As at this depth. Aqueous As was only 4 ± 1 μg/L in the one well in the lower aquifer (165 m). Aqueous As did not appear to be associated with suspended particulate material greater than 50 nm; As in the unfiltered, 200 nm, and 50 nm filtered fractions were within the analytical error of each other for most depths (Fig. 3a).

The majority of As in the 50 nm filtered samples at most depths (>80% between 14 and 61 m) appears to be As(III) (Fig. 3b). No strong depth dependence in the percent As(III) is apparent, although waters with the lowest aqueous As concen-

Table 2. Aqueous parameters.

Measurement (units)	Well depth (m)														
	4.6	9.1	14	18	24	30 (1)	30 (2)	30 (3)	38	46	61 (1)	61 (2)	76	107	165
pH	6.63	6.71	6.80	6.81	6.86	7.01	6.94	6.87	7.00	7.00	6.94	6.95	6.93	7.10	6.82
redox electrode (mV)[a]	65	88	83	79	40	23	79	74	95	35	61	26	24	69	90
dissolved O_2 (mg/L)[a]	nd[b]	nd	0.33	nd	nd	nd	nd	nd	nd	nd	nd	nd	nd	nd	nd
conductivity (μS/cm)[a]	529	480	414	554	676	803	787	755	924	1000	975	763	1010	1240	1900
As total unfilt. (μg/L)[c]	6.3 ± 0.7[d]	6.1 ± 1.0[d]	70 ± 0.1[e]	200 ± 5.2[e]	340 ± 12[e]	640 ± 19[e]	490 ± 4.0[e]	380 ± 1.1[e]	540 ± 4.0[e]	360 ± 16[e]	220 ± 5.7[e]	110 ± 1.8[e]	44 ± 6.7[e]	58 ± 2.9[e]	4.1 ± 0.7[d]
As 200 nm filt. (μg/L)[c]	4.7 ± 1.0[d]	9.4 ± 3.0[d]	78 ± 1.3[e]	210 ± 5.2[e]	350 ± 41[e]	640 ± 38[e]	480 ± 7.4[e]	360 ± 4.8[e]	560 ± 9.9[e]	360 ± 22[e]	85 ± 7.7[e]	110 ± 8.9[e]	34 ± 4.7[e]	35 ± 2.9[e]	6.4 ± 1.2[d]
As 50 nm filt. (μg/L)[c]	4.4 ± 0.1[d]	6.8 ± 0.1[d]	72 ± 2.2[e]	220 ± 5.2[e]	390 ± 12[e]	660 ± 0.1[e]	460 ± 0.7[e]	340 ± 17[e]	570 ± 11[e]	350 ± 16[e]	72 ± 1.8[e]	96 ± 12[e]	29 ± 3.1[e]	45 ± 9.2[e]	5.4 ± 3.1[d]
As(III) (%)[f]	47[g]	45 ± 4.3	79 ± 2.3	92 ± 1.0	96 ± 8.3	87 ± 1.8	91 ± 0.1	85 ± 0.1	89 ± 0.9	81 ± 0.3	81 ± 0.6	78 ± 1.6	62 ± 1.2	89 ± 1.3	35 ± 40
NH_4^+-N (mg/L)[h]	0.7 ± 0.1	0.7 ± 0.1	6.5 ± 1.0	7.5 ± 1.0	9.0 ± 1.0	8.5 ± 1.0	9.0 ± 1.0	6.5 ± 1.0	12 ± 1.0	4.5 ± 1.0	3.5 ± 1.0	3.5 ± 1.0	3.5 ± 1.0	1.5 ± 1.0	0.5 ± 0.1
NO_3^--N (mg/L)[h]	nd	nd	nd	nd	nd	nd	nd	nd	nd	nd	nd	nd	nd	nd	nd
Fe(II) (mg/L)[h]	7.5 ± 1.0	3.5 ± 1.0	5.5 ± 1.0	4.5 ± 1.0	10 ± 1.0	10 ± 1.0	3.0 ± 1.0	5.5 ± 1.0	1.5 ± 1.0	5.5 ± 1.0	3.5 ± 1.0	4.5 ± 1.0	9.0 ± 1.0	1.5 ± 1.0	1.5 ± 1.0
Fe_{total} (mg/L)[h]	7.5 ± 1.0	3.5 ± 1.0	5.5 ± 1.0	4.5 ± 1.0	10 ± 1.0	10 ± 1.0	3.0 ± 1.0	5.5 ± 1.0	1.5 ± 1.0	5.5 ± 1.0	3.5 ± 1.0	4.5 ± 1.0	9.0 ± 1.0	1.5 ± 1.0	1.5 ± 1.0
Mn(II) (mg/L)[h]	0.5 ± 0.1	0.7 ± 0.1	0.1 ± 0.1	0.9 ± 0.1	1.2 ± 0.5	1.6 ± 0.5	1.0 ± 0.5	2.0 ± 0.5	0.4 ± 0.1	0.2 ± 0.1	0.9 ± 0.1	1.2 ± 0.5	0.9 ± 0.1	0.2 ± 0.1	0.2 ± 0.1
SO_4^{2-} (mg/L)[a]	36	22	18	10.6	0.6	0.1	0.2	2.7	0.2	0.2	0.2	0.6	0.8	11	46
$sulfide_{total}$ (μg/L as S)[h]	64	64	nd	nd	nd	nd	nd	nd	nd	nd	64	nd	nd	nd	nd
DOC (mg/L)[c]	3.1 ± 0.1	3.9 ± 0.2	5.2 ± 0.3	4.3 ± 0.1	6.3 ± 0.1	12 ± 1.3	8.2 ± 0.5	12 ± 1.2	11 ± 0.2	6.0 ± 0.1	11 ± 0.3	15 ± 0.3	12 ± 0.9	7.9 ± 0.1	3.4 ± 0.1
HCO_3^- (mg/L) (titration)[a]	170	230	220	270	360	420	430	410	490	550	520	390	570	550	350
HCO_3^- (mg/L) (headspace)[a]	185	155	nm[i]	340	nm	nm	nm	nm	600	nm	720	nm	480	nm	390
$phosphate_{total}$ (mg/L)[h]	3.5 ± 1.0	2.5 ± 1.0	6.5 ± 1.0	4.5 ± 1.0	5.5 ± 1.0	5.5 ± 1.0	2.5 ± 1.0	3.5 ± 1.0	4.5 ± 1.0	6.5 ± 1.0	4.5 ± 1.0	5.5 ± 1.0	5.5 ± 1.0	2.5 ± 1.0	3.5 ± 1.0
$silicon_{total}$ by GFAA (mg/L as SiO_2)[c]	37 ± 1	40 ± 1	54 ± 2	44 ± 2	41 ± 1	40 ± 3	41 ± 3	37 ± 1	42 ± 1	44 ± 1	42 ± 1	35 ± 1	39 ± 1	38 ± 1	43 ± 1
molybdate-reactive silica (mg/L as SiO_2)[c]	41	41	61	48	40	37	36	34	41	48	43	37	43	37	59
Ca_{total} (mg/L)[c]	35 ± 0.8	28 ± 0.6	38 ± 0.9	54 ± 1.6	67 ± 1.8	98 ± 2.5	86 ± 2.5	84 ± 2.4	99 ± 2.9	84 ± 2.4	27 ± 0.7	41 ± 1.2	20 ± 0.5	19 ± 0.5	44 ± 1.9
Mg_{total} (mg/L)$_c$	19 ± 1.6	18 ± 1.5	14 ± 1.5	17 ± 1.5	20 ± 1.6	21 ± 0.7	24 ± 1.7	24 ± 1.7	17 ± 1.5	49 ± 2.2	28 ± 1.8	37 ± 2.0	35 ± 1.9	22 ± 1.7	22 ± 1.7
Na_{total} (mg/L)$_c$	16 ± 1.0	30 ± 1.8	8.9 ± 0.6	11 ± 0.7	15 ± 0.9	17 ± 1.2	16 ± 1.0	23 ± 1.4	22 ± 1.3	26 ± 1.5	20 ± 1.2	31 ± 1.7	32 ± 1.7	89 ± 6.3	280 ± 16
K_{total} (mg/L)$_c$	2.5 ± 0.1	2.9 ± 0.1	4.0 ± 0.1	5.2 ± 0.2	6.5 ± 0.7	8.1 ± 1.2	7.9 ± 0.7	9.1 ± 0.7	7.2 ± 0.7	8.7 ± 0.7	5.8 ± 0.4	11 ± 0.5	7.5 ± 0.4	6.5 ± 0.4	6.9 ± 0.7
Cl_{total} (mg/L)[c]	20	19	13	17	8.4	8.5	11	22	28	22	22	25	23	53	390

[a] Represents one measurement.

[b] nd = not detected (detection limits: dissolved O_2, 0.3 mg/L; dissolved sulfide, 25 μg/L; NO_3-N, 0.05 mg/L).

[c] Average ± 1 stnd. dev. of two or more aliquots of one collected sample.

[d] Measured by HGFS (150 ng/L detection limit).

[e] Measured by GFAA (5 ng/L detection limit).

[f] Average ± 1 stnd. dev. of two collected samples.

[g] One of two collected samples lost to spillage

[h] Represents one chemet measurement ± increment in chemet scale.

[i] nm = not measured.

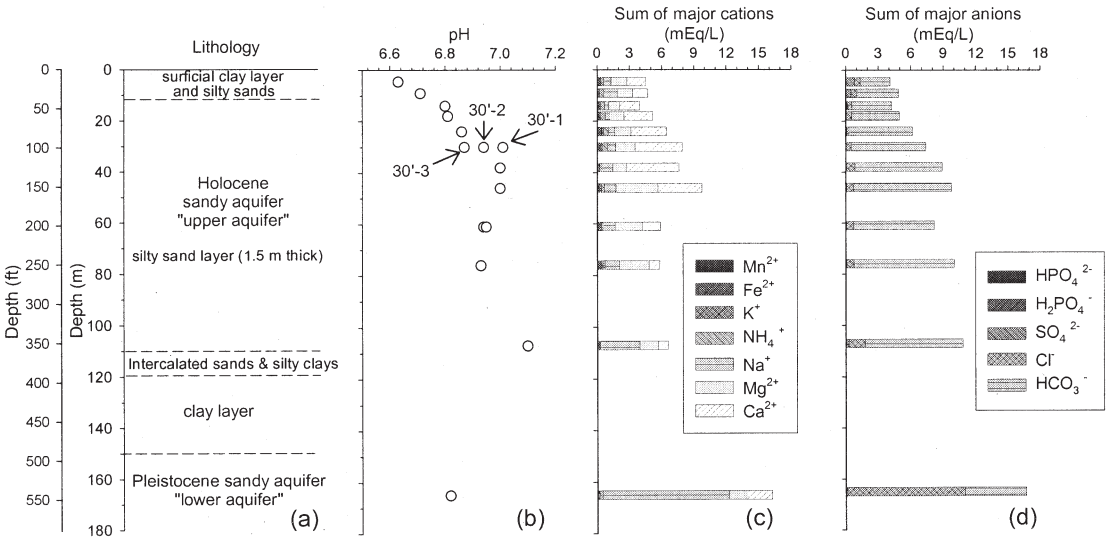

Fig. 2. Depth profiles of (a) the lithologies encountered to 165 m; (b) pH; and the sum of major (c) cations (in mEq/L), and (d) anions (in mEq/L). The sums of major cations and anions are typically within 5% of each other except for the 61, 76 and 107 m depths, where the charge of measured cations is only approximately 60 to 75% of charge of measured anions.

trations (4.6 m, 9.1 m, and the 165 m) exhibit a somewhat lower percent As(III) (Fig. 3b). Method recovery experiments suggest, though, that the lower fraction As(III) measured for these depths may be due, in part, to disproportionate loss of As(III) to the resin from samples that were not acidified before separation and that have lower (i.e., <10 μg/L) total As concentrations. We found that losses of total As(III) to the resin from unacidified (pH 5 to 6) standards containing 5 μg/L As(III) were 27 $\pm$ 13%, while acidified 5 μg/L standards lost only 2.0 $\pm$ 1.7% and unacidified 1 mg/L As(III) standards lost only 0.4 $\pm$ 0.3% of the total As(III) to the resin.

Solid phase As concentrations exhibit little depth dependence and are typically less than 2 μg/g (Fig. 4a), although in the surficial clay layer and in the deeper clay layer at 119 to 150 m, concentrations are somewhat greater (3 to 8 μg/g). Sediment at 31 m, a depth within the range exhibiting the greatest aqueous As levels (Fig. 3a), also shows s somewhat higher solid phase As concentration (4.0 $\pm$ 0.7 μg/g) (Fig. 4a).

3.2.3. Redox components

The predominance of As(III) in the aqueous phase is consistent with other geochemical indicators of suboxic to anoxic conditions in the upper and lower aquifers. Dissolved O_2 concentrations were below the approximate detection limit of 0.3 mg/L, with the exception of only one depth (0.33 mg/L at 14 m; Table 2). Platinum electrode measurements fell in a narrow range from 20 mV to 100 mV (corrected to the standard hydrogen electrode) (Table 2). Consistent with the very low levels of oxygen and low platinum electrode measurements, no NO_3^--N was detected in the aqueous samples, while NH_4^+-N was present and had a peak concentration of 12 mg/L at the 38 m depth (Fig. 3c). Dissolved Fe(II) levels (Fig. 3d), indistinguishable from total dissolved Fe, ranged from 1.5 to 10 mg/L with no apparent systematic depth dependence, similar to total solid phase Fe levels (Fig. 4b). Mn(II) was also detected throughout the profile at concentrations from 0.1 mg/L to 2.0 mg/L (Fig. 3e), with the most elevated levels measured in the 30 and 38 m wells.

Dissolved sulfur was mostly present as sulfate, with the highest concentrations (36 and 46 mg/L) occurring at the shallowest depth in the upper aquifer and in the one well in the lower aquifer, respectively (Fig. 3f). Sulfate levels were typically below 1.0 mg/L throughout much of the profile. While dissolved sulfide exceeded the detection limit (25 μg/L) in only three wells, all in the upper aquifer (Table 2), approximately 10% of total sulfur in the sediments appears to be incorporated in AVS (compare Figs. 4c,d).

Dissolved organic carbon (DOC) increases from 3.1 mg/L in the shallow wells to 11 mg/L or greater at depths of 30 to 76 m in the upper aquifer (Fig. 3g). Bicarbonate (HCO_3^-) covaries with dissolved organic carbon (DOC), but is 10 or more times larger in concentration (160 to 570 mg/L) (Fig. 3h).

Total solid phase carbon is typically between 0.1 to 1.0 mg/g sediment, while inorganic carbon is at most 25% of the total solid phase carbon (Fig. 4e). Such low solid phase carbon levels are consistent with the failure to observe peat layers in this core, although peat deposits have been postulated as possible sources of DOC observed in Bangladesh and Vietnamese aquifers (Berg et al., 2001; McArthur et al., 2001). It is possible that a thin (less than 61 cm thick) peat layer could exist in the profile, although no such layers were found by visual inspection. It is also possible that discontinuous horizontal peat layers exist in the subsurface at the Munshiganj site but were not penetrated at the coring location.

3.3. Extraction Data

3.3.1. As

Concentrations (in ng/g sediment) of operationally defined fractions of solid phase As leached cumulatively by the MG and

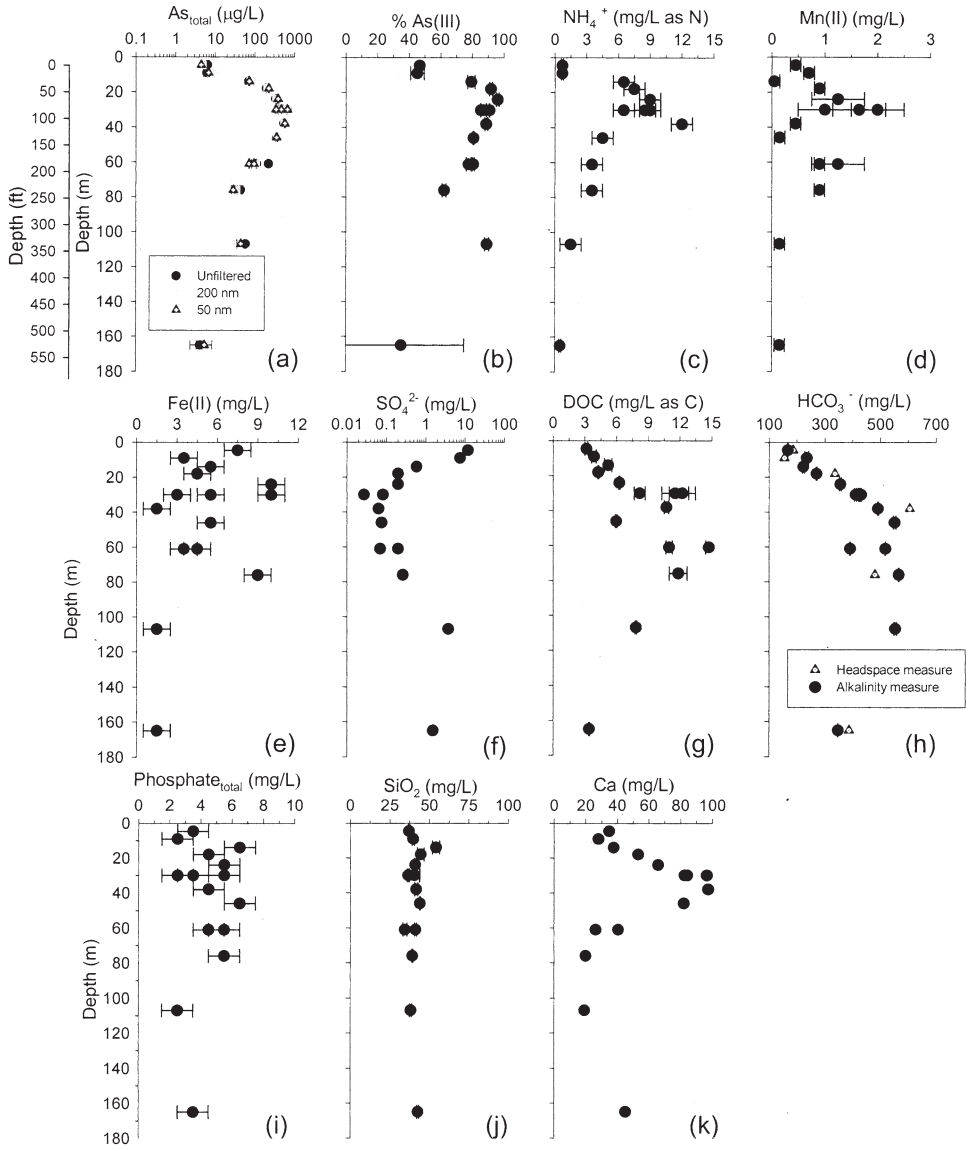

Fig. 3. Depth profiles of aqueous constituents, including (a) As concentrations categorized as unfiltered, 200 nm filtered, and 50 nm filtered fractions in μg/L; (b) the percent As(III) in 50 nm filtered fractions; (c) NH_4^+ in mg/L as N; (d) Mn(II) in mg/L; (e) Fe(II) in mg/L; (f) SO_4^{2-} in mg/L; (g) DOC in mg/L; (h) bicarbonate, in mg/L, inferred from alkalinity and calculated from measurement of CO_2 in the headspace of syringe samples; (i) total Ca in mg/L; (j) total phosphate in mg/L; and (k) silicon measured by GFAA, as mg/L SiO_2. Error bars are defined in Table 2.

PHOS extractants (interpreted as adsorbed) and the HCl and OX extractants (interpreted as coprecipitated in solids, possibly AVS, carbonates, phosphates, mixed valence and amorphous oxides) covary with depth, although the range in concentrations for either pool generally spans less than one order of magnitude (Fig. 5; see Table 3 for concentrations of As in each pool). As extracted by the pH 2 solution (also interpreted as adsorbed) is presented also in Figure 5 for comparison with the sum of As in the MG and PHOS extracts; As extracted by the pH 2 extractant was 80 ± 37% of the sum of As in the MG and PHOS extracts (see Table A1 in the Appendix for pH 2 extraction data). Note that the amounts of As in these pools of As, relatively mobile under reducing conditions, are similar throughout the depth profile, being only a factor of 2 to 4 less in the lower aquifer, where aqueous As is 4 μg/L, than in sediments at depths of 30 to 38 m in the upper aquifer, where aqueous As is greater than 400 μg/L (Fig. 2c). Note also that the sum of MG and PHOS As is only 1 to 10 times larger than aqueous As (assuming a porosity of 0.3 and a solids' density of 2.6 g/cm^3).

As a proportion of total solid phase As, the amounts of As in the MG, PHOS, HCl and OX pools also vary little with depth, cumulatively accounting for 20 to 50% of total solid phase As (Table 3). Most of the remaining As was found in the HF, NIT and HOT NIT extracts and may be As incorporated in more recalcitrant phases such as silicate minerals and crystalline sulfides (Huerta-Diaz and Morse, 1992; Keon et al., 2001). The sum of total solid As recovered from all extraction steps (Table 3) was comparable to total solid As measured by XRF (130 ± 58%).

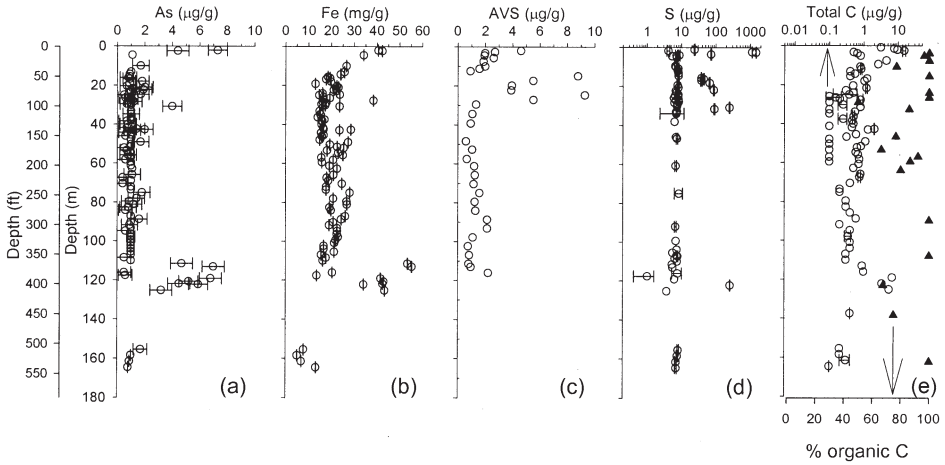

Fig. 4. Depth profiles of solid phase constituents, including (a) As in μg/g, (b) Fe in mg/g, (c) AVS in μg/g, (d) total sulfur in μg/g, and (e) total carbon in mg/g on the upper axis and percent organic carbon on the lower axis. Error bars, present for the As, Fe, total S, and total C, represent one standard deviation for two replicate analyses.

3.3.2. *Fe*

The proportions of solid phase Fe extracted in the HCl and OX steps are fairly constant with depth, each constituting approximately 5 to 10% of total solid phase Fe (Table 4). The oxidation state(s) of the Fe liberated in the HCl step was determined in sediments from depths of 24.7, 25.9, 29.0, and 30.2 m taken from the core obtained in January 2002; essentially all of the HCl-extractable Fe was Fe(II) (106 ± 3%, data not shown). The fraction of Fe(II) in HCl extracts for two older sediment samples (from 29.5 m and 30.8 m, taken from the April 2000 core) and extracted concurrently with the fresher core samples was 90 ± 7.1% (data not shown), indicating that some oxidation had occurred over the 2-yr storage time of these core samples (all samples were kept frozen in sealed containers even after completion of all other extraction experiments performed on aliquots of these samples a year earlier).

TiCEB-extractable Fe in the sediments is typically 10 to 20% of solid phase Fe (Table 4), with sediments from the lower aquifer (165 m) containing the largest percentage of TiCEB-extractable Fe (30%). This finding is consistent with the brown to orange coloring of sediments from lower aquifer, which suggests the presence of Fe(III) oxyhydroxides.

The majority of solid phase Fe (60 to 80%; Table 4) is extractable only by HF, NIT and HOT NIT, and is likely Fe incorporated in silicate minerals, pyrite, and perhaps Fe-Ti phases. Recovery of total solid Fe from all extraction steps (Table 4), calculated by comparing the sum of Fe recovered in all extraction steps to total Fe measured by XRF, was 95 ± 18% for all the depths analyzed.

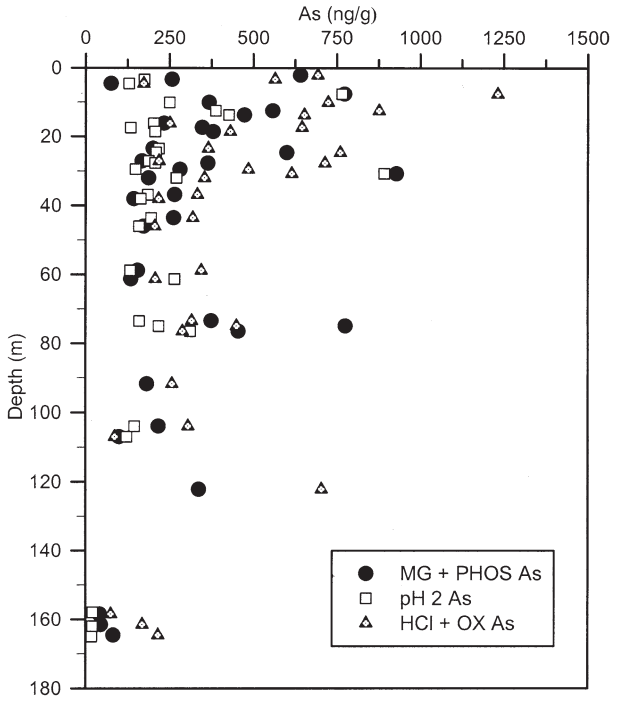

Fig. 5. Depth profiles of pH 2-extractable As, the sum of MG- and PHOS-extractable As, and the sum of HCl and OX extractable As, all in ng/g sediment. Refer to text for detailed descriptions of extractants. The pH 2, MG, and PHOS pools of As are interpreted to be adsorbed; HCl- and OX-extractable As is interpreted as coprecipitated in solids.

3.5. As Associations with Solid Phases

3.5.1. *Indications from extraction results*

As interpreted as adsorbed (MG- and PHOS-extractable, or pH 2-extractable) and the sum of As liberated by the HCl, OX, and TiCEB extractants are all positively correlated with the sum of solid phase Fe measured in the HCl, OX, and TiCEB extracts (Fig. 6). Cumulative As leached by the HCl, OX, and TiCEB extractants is better correlated ($R^2 = 0.65$, $p = 0.001$, i.e., significant at the 99.9% confidence level) with the Fe in these pools than As liberated by the MG and PHOS ($R^2 = 0.42$, $p = 0.005$) or pH 2 ($R^2 = 0.27$, $p = 0.055$, not significant) extractants. The regressions of extracted As with extracted Al indicate a much poorer correlation of As to Al than As to Fe. The statistics for As in the MG and PHOS pools ($R^2 = 0.03$, $p = 0.044$); pH 2 extract ($R^2 = 0.001$, $p = 0.916$, not signifi-

Table 3. Sequential extraction and XRF data for As (ng/g).

Depth (m)	MG	PHOS	HCl	OX	TiCEB	HF	NIT + HOT NIT	Extraction total	XRF total
2.1	24 (0.4)[a]	620 (11)	180 (3.2)	510 (9.1)	560 (10)	780 (14)	2940 (52)	5610	7300
3.4	33	220	180	390	nm[b]	nm	nm	—	nm
4.6	11 (0.6)	64 (3.3)	43 (2.2)	130 (6.5)	53 (2.7)	810 (41)	860 (44)	1970	1100
7.6	110	660	490	740	nm	nm	nm	—	nm
10.1	6.1 (0.2)	360 (14)	200 (7.8)	520 (20)	310 (12)	620 (24)	590 (23)	2610	1700
12.5	29	530	270	600	nm	nm	nm	—	nm
13.7	20	450	210	440	nm	nm	nm	—	nm
16.2	nd[c] (0.0)	230 (18)	140 (11)	110 (9.0)	100 (8.1)	87 (6.8)	600 (47)	1270	900
17.4	31	320	220	430	nm	nm	nm	—	nm
18.6	17	360	170	270	nm	nm	nm	—	nm
23.5	27	170	170	200	nm	nm	nm	—	nm
24.7	40	560	310	450	nm	nm	nm	—	nm
27.1	4.6 (0.4)	160 (14)	98 (8.1)	120 (10)	60 (5.0)	600 (50)	150 (13)	1200	1000
27.7	nd (0.0)	360 (24)	180 (12)	530 (35)	94 (6.2)	160 (11)	190 (13)	1510	1100
29.5	13	270	170	320	nm	nm	nm	—	nm
30.8	33 (1.0)	900 (26)	110 (3.2)	500 (15)	180 (5.3)	850 (25)	830 (24)	3400	4000
32.0	5.9 (0.4)	180 (13)	64 (4.5)	290 (20)	82 (5.8)	650 (46)	150 (10)	1420	nm
36.9	24	240	130	200	nm	nm	nm	—	nm
38.1	14 (0.8)	130 (7.2)	45 (2.5)	170 (9.6)	56 (3.1)	610 (34)	770 (43)	1800	1000
43.6	21.1	240	120	200	nm	nm	nm	—	nm
46.0	4.5 (0.3)	200 (11)	67 (3.9)	170 (9.8)	86 (4.9)	950 (54)	280 (16)	1760	600
58.8	10	140	84	260	nm	nm	nm	—	nm
61.3	13 (0.9)	150 (10)	72 (5.0)	170 (12)	62 (4.3)	770 (53)	210 (15)	1450	1000
73.5	160	170	110	170	nm	nm	nm	—	nm
75.0	16	640	150	230	nm	nm	nm	—	nm
76.5	170 (8.0)	270 (12)	48 (2.2)	230 (11)	140 (6.5)	920 (42)	390 (18)	2170	nm
91.7	7.2 (1.0)	180 (24)	96 (13)	160 (22)	50 (6.9)	98 (14)	130 (19)	720	900
104	24	190	120	190	nm	nm	nm	—	nm
107	5.3 (0.6)	95 (11)	27 (3.1)	61 (7.0)	100 (12)	490 (56)	90 (10)	870	1000
122	nd (0.0)	340 (12)	180 (6.3)	520 (18)	180 (6.3)	630 (22)	1000 (35)	2850	2500
158	8.1 (0.9)	34 (3.7)	2.0 (0.2)	74 (8.0)	76 (8.2)	360 (38)	380 (41)	930	1000
162	nd	45	16	150	nm	nm	nm	—	nm
165	1.3 (0.2)	81 (16)	2.6 (0.5)	210 (41)	94 (18)	86 (17)	43 (8.3)	520	800

[a] As in ng/g with percent of total extracted in parentheses for samples where all extraction steps were conducted.
[b] Not measured.
[c] Not detected (<1.0 ng/g).

cant); and HCl, OX, and TiCEB extracts ($R^2 = 0.13$, $p = 0.539$, not significant) all indicate a weaker correlation with solid phase Al liberated by the HCl, OX, and TiCEB extracts, which is present at concentrations averaging 70% of Fe on a molar basis (data not shown).

3.5.2. *Microprobe elemental mapping*

Microprobe analyses of sediment samples taken from 29.5 m in the upper aquifer and 165 m in the lower aquifer indicated that As and Fe covary spatially within the sediments' fine-grained constituents (Figs. 7a,b). Fe and As fluorescence intensities were highly correlated ($R^2 = 0.79$) in a mapped area of sediment taken from the 29.5 m depth (Fig. 7a). For the 165 m sample, Fe and As intensities were less correlated when considering the regression statistic ($R^2 = 0.27$; Fig. 7b) generated by including the entire data set; however, As intensities are relatively independent of Fe intensities in two smaller subsets of the data in Figure 7b (indicated with arrows), with most of the remaining majority of data points falling along a single trend line. This suggests that much of the As covaries spatially with Fe in this sample also.

The As and Fe fluorescence intensities correspond approximately to As/Fe molar ratios of 2×10^{-4} and 1×10^{-4} for the 29.5 and 165 m samples, respectively, after applying an approximate relative sensitivity factor of 70 for As (Sutton, private communication, 2001) to the regression slopes for the fluorescence data. These microprobe-derived molar ratios are within factors of four and two of the As/Fe molar ratios (3×10^{-5} and 5×10^{-5}) determined from XRF analyses of samples from comparable depths (29.6 and 165 m, respectively).

3.5.3. *Analyses of density and magnetic separates*

The mineralogy found in comparable (where analyzed) density/magnetic fractions from the 27.7 m, 74.7 m, and 165 m depths are generally similar. For all depths, quartz dominates the XRD spectrum of the <2.85 g/cm^3 fraction, with lesser and similar amounts of the feldspars, albite and microcline, and micas (Table 5), although quartz is substantially more abundant in the 165 m depth fraction. The hand-magnetic fraction spectrum comprises almost entirely magnetite (98%) for the 27.7 m depth (insufficient sample was available to perform similar analysis with the 74.7 m and 165 m depths). Assuming amorphous solids compose only a minor portion of the hand-magnetic fraction, the XRD results, relative abundance (Table 6),

Table 4. Sequential extraction and XRF data for Fe (mg/g).

Depth (m)	MG	PHOS	HCl	OX	TiCEB	HF	NIT+HOT NIT	Extraction total	XRF total
2.1	nd[a] (0.0)[b]	0.2 (0.5)	5.8 (13)	2.7 (6.0)	2.6 (5.9)	29 (65)	4.1 (9.3)	44	41
3.4	nm[c]	nm	4.3	3.4	nm	nm	—	nm	
4.6	nd (0.0)	1.4 (4.1)	5.1 (15)	2.0 (6.0)	0.3 (0.9)	20 (59)	5.1 (15)	34	34
7.6	nm	nm	6.8	3.3	nm	nm	nm	—	nm
10.1	nd (0.0)	0.9 (2.9)	12 (41)	1.8 (5.9)	0.4 (1.2)	13 (42)	2.3 (7.6)	30	27
12.5	nm	nm	2.8	3.7	nm	nm	nm	—	nm
13.7	nm	nm	1.9	1.4	nm	nm	nm	—	nm
16.2	nd (0.0)	0.2 (1.5)	1.2 (7.6)	1.0 (6.7)	1.3 (8.6)	9.7 (63)	2.1 (13)	16	18
17.4	nm	nm	9.0	1.5	nm	nm	nm	—	nm
18.6	nm	nm	0.9	7.1	nm	nm	nm	—	nm
23.5	nm	nm	1.4	0.8	nm	nm	nm	—	nm
24.7	nm	nm	2.5	2.4	nm	nm	nm	—	nm
27.1	nd (0.0)	0.2 (1.4)	0.9 (6.2)	0.8 (5.6)	1.1 (7.8)	9.4 (65)	2.1 (14)	15	16
27.7	nd (0.0)	0.2 (0.7)	1.2 (5.8)	1.5 (7.0)	1.8 (8.1)	14 (63)	3.3 (15)	22	38
29.5	nm	nm	0.8	0.8	nm	nm	nm	—	nm
30.8	nd (0.0)	1.2 (4.1)	9.6 (32)	2.1 (7.0)	0.5 (1.6)	14 (48)	2.4 (7.9)	30	24
32.0	nd (0.0)	0.4 1.2 ()	1.1 (3.6)	1.1 (3.6)	0.3 (1.0)	22 (75)	4.6 (16)	30	nm
36.9	nm	nm	0.9	0.8	nm	nm	nm	—	nm
38.1	nd (0.0)	0.3 (1.7)	0.9 (4.8)	0.8 (4.7)	0.2 (1.3)	11 (62)	4.4 (25)	18	16
43.6	nm	nm	1.1	0.7	nm	nm	nm	—	nm
46.0	nd (0.0)	0.2 (1.5)	1.3 (8.8)	0.8 (5.1)	1.5 (9.7)	9.1 (61)	2.1 (14)	15	16
58.8	nm	nm	0.9	0.7	nm	nm	nm	—	nm
61.3	nd (0.0)	0.3 (1.5)	1.4 (8.1)	1.0 (6.0)	1.5 (8.7)	10 (57)	3.2 (18)	17	19
73.5	nm	nm	1.3	0.7	nm	nm	nm	—	nm
75.0	nm	nm	1.4	0.7	nm	nm	nm	—	nm
76.5	nd (0.0)	0.4 (1.7)	1.5 (6.0)	1.0 (4.0)	0.5 (2.1)	15 (63)	5.6 (23)	24	nm
91.7	nd (0.0)	0.2 (1.2)	1.5 (8.5)	1.1 (6.4)	1.4 (8.2)	11 (61)	2.6 (15)	17	19
104	nm	nm	1.5	1.1	nm	nm	nm	—	nm
107	nd (0.0)	0.2 (1.7)	1.0 (9.2)	0.5 (4.6)	1.9 (17)	6.5 (59)	1.0 (9.0)	11	16
122	nd (0.0)	0.1 (0.3)	3.6 (12)	2.7 (9.0)	4.8 (16)	16 (56)	2.0 (6.6)	30	34
158	nd (0.0)	0.1 (1.6)	0.8 (8.7)	0.7 (7.9)	0.1 (0.8)	6.7 (72)	0.8 (8.9)	9	8.5
162	nm	nm	1.1	1.2	nm	nm	nm	—	nm
165	nd (0.0)	0.1 (0.9)	0.9 (7.4)	1.7 (13)	3.7 (30)	5.1 (41)	1.0 (7.8)	12	13

[a] Not detected (<0.5 μg/g).
[b] Fe in mg/g with percent of total extracted in parentheses for samples where all extraction steps were conducted.
[c] Not measured.

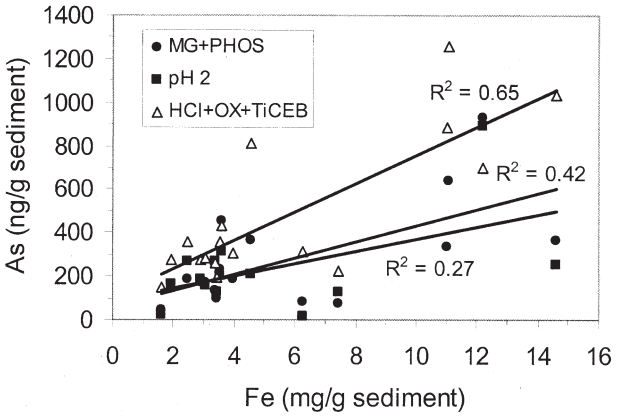

Fig. 6. Correlations between the sum of As liberated cumulatively by the MG and PHOS steps ($R^2 = 0.42$) or by the pH 2 extractant ($R^2 = 0.27$) (both interpreted as adsorbed, ng/g sediment) and the sum of Fe in the HCl, OX, and TiCEB extracts (mg/g sediment); and between the sum of As (ng/g sediment) and Fe (mg/g sediment) liberated by HCl, OX, and TiCEB steps (in mg/g sediment dry weight) ($R^2 = 0.65$).

and NAA analysis for this fraction for the 27.7 m depth suggest that the Fe contained therein (490 mg/g fraction, Fig. 8a) can account for approximately 80% of the OX-extractable Fe found in samples of the bulk sediment (1.5 mg OX Fe/g for 27.7 m, Table 4). This is consistent with the fact that oxalic acid is known to effectively dissolve magnetite (Canfield and Berner, 1987; Canfield, 1989). The 0.5 amp fraction consists largely of hornblende (53 to 55%) in the two depths, while the 1.0–1.5 amp fraction is predominantly muscovite (33 to 46%) and amphibole (approximately 30%) (Table 5). The nonmagnetic fraction consists of several accessory minerals (apatite, titanite, rutile, and zircon) and the metamorphic minerals sillimanite and kyanite. Pyrite is present at only 0.3 ± 0.1% by weight of the nonmagnetic fraction of the 27.7 m depth, consistent with observations made in other Bangladesh sediments (Nickson et al., 2000).

NAA analyses of density and magnetic separates for As indicate that the hand-magnetic fraction typically has a larger As concentration than the other fractions for all four depths analyzed (including the 165 m depth from the lower aquifer) (Fig. 8b). It was not ascertained whether this As was associated directly with the magnetite that is predominant in this fraction,

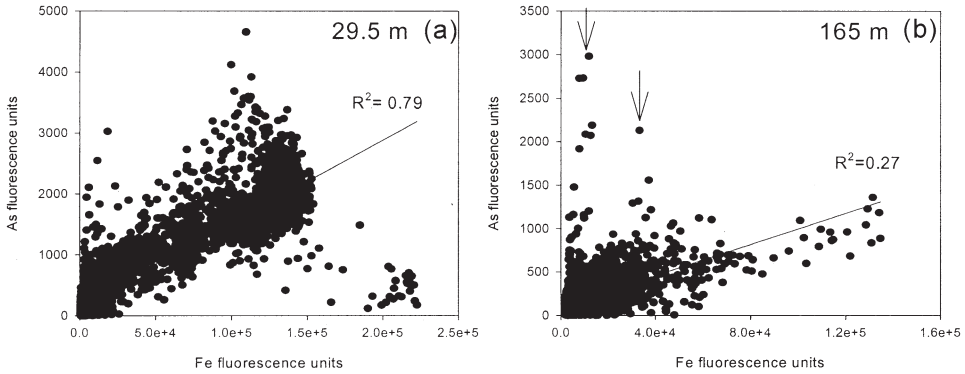

Fig. 7. Correlations between microprobe-mapped X-ray fluorescence intensities for solid phase As and Fe from a 400 × 340 μm area of sample taken from (a) 29.5 m in the shallow aquifer ($R^2 = 0.79$), and (b) 165 m in the deeper aquifer ($R^2 = 0.27$). The arrows in (b) point to subsets of data in which As and Fe concentrations do not covary spatially.

or with Fe-rich coatings on the magnetite. Fe-rich coatings are ubiquitous on other mineral constituents such as quartz and aluminosilicate phases in all fractions from 27.7 m, as observed with SEM (see Fig. 9, for example). Indeed, such coatings may explain why most of the solid phase As in the bulk sediment is associated with the <2.85 g/cm^3 fraction, which is dominated by quartz and feldspars (Table 5).

4. DISCUSSION

4.1. Mechanisms Controlling As Mobility

4.1.2. Prior As release due to reductive dissolution of Fe(III) oxyhydroxides

Solid phase As concentrations (Fig. 4a) measured in both the upper and lower aquifer sediments at this site are comparable to those measured in sediments collected in other As-affected districts in Bangladesh, such as Lakshimpur, Faridpur, Chapai Nawabganj, and Gopalganj (Nickson et al., 2000; BGS & DPHE, 2001). Similar levels of solid phase As have been found also in Vietnamese alluvial aquifers with comparably elevated dissolved As levels (Berg et al., 2001). These solid phase As concentrations, indistinguishable from average crustal abundances of As (Cullen and Reimer, 1989; Smedley and Kinniburgh, 2002), indicate that the high dissolved As concentrations in the upper aquifer (Fig. 3a) are not due to particularly elevated solid phase As concentrations in the sediments, as noted by others (Nickson et al., 2000; McArthur et al., 2001; BGS & DPHE, 2001). Rather, the suboxic to anoxic conditions, presence of dissolved Fe(II), and general correspondence between dissolved As, NH_4^+, and HCO_3^- at this site (compare

Table 5. Mineralogy of density/magnetic separates.

Depth (m)		>2.85 g/cm^3			
	<2.85 g/cm^3	Hand magnet	0.5 amp	1.0 + 1.5 amp	Nonmagnetic
27.7	quartz (66 ± 1)[a] albite (15 ± 1) microcline (13 ± 1) muscovite (5.6 ± 0.3)	magnetite (98 ± 2) quartz (2.1 ± 0.6)	hornblende (55 ± 2) epidote (16 ± 1) garnet (13 ± 1) muscovite (9.1 ± 1.4) quartz (6.5 ± 0.3)	muscovite (46 ± 6) amphibole (32 ± 4) biotite (21 ± 3) chlorite (1.2 ± 0.7)	silimanite (30 ± 1) apatite (20 ± 1) kyanite (17 ± 1) quartz (14 ± 1) titanite (12 ± 1) rutile (3.2 ± 0.4) zircon (2.8 ± 0.2) pyrite (0.3 ± 0.1)
74.7	quartz (61 ± 1) albite (20 ± 0.4) microcline (12 ± 0.4) muscovite (5.7 ± 0.5) biotite (1.4 ± 0.3)	nm[b]	hornblende (53 ± 2) epidote (25 ± 1) biotite (10 ± 1) quartz (6.7 ± 0.5) garnet (5.7 ± 0.7)	muscovite (33 ± 4) amphibole (29 ± 4) quartz (18 ± 1) apatite (16 ± 2) zircon (4.4 ± 0.5)	epidote (20 ± 1) quartz (16 ± 1) titanite (15 ± 1) sillimanite (13 ± 1) amphibole (12 ± 1) albite (8.1 ± 0.8) biotite (6.6 ± 0.5) apatite (4.8 ± 0.6) kyanite (2.4 ± 0.6) garnet (2.2 ± 0.7)
165	quartz (81 ± 1) microcline (12 ± 1) albite (5.4 ± 0.3) muscovite (1.3 ± 0.3)	nm	nm	nm	nm

[a] Weight fraction ± one standard deviation. Reported weight fractions are dependent on the composition of the model phases used in fitting the data and are normalized to 100%. Standard deviation reflects counting statistics.

[b] Not measured due to insufficient sample quantity.

Table 6. Relative abundances of density/magnetic separates.

Fraction	Percent of bulk sediment			
	9.4 m	27.7 m	74.7 m	165 m
<2.85 g/cm^3	82.78	92.53	95.76	95.60
>2.85 g/cm^3				
Hand magnet	0.04	0.25	0.15	0.54
0.5 amp	2.22	5.24	3.03	2.55
1.0 ± 1.5 amp	0.31	0.70	0.46	0.42
Nonmagnetic	0.40	0.52	0.28	0.55

Figs. 3a,c,h) are consistent with the mechanism of reductive dissolution of Fe(III) oxyhydroxides via respiration of organic matter, with concomitant release of associated adsorbed and coprecipitated As, as has been indicated elsewhere in Bangladesh and other locales (Shimada, 1996; Bhattacharya et al., 1997; Nickson et al., 2000, Welch et al., 2000; Berg et al., 2001; BGS & DPHE, 2001).

As noted by Harvey et al. (2002), the close correspondence between the aqueous As and Ca profiles (compare Figs. 3a and 3i) may indicate that dissolution of calcite accompanied this release of As, driven by CO_2 generated from the respiration process (Jakobsen and Postma, 1999). Calcite is near equilibrium to slightly supersaturated with the aqueous phase throughout much of the depth profile (Fig. 10), and inorganic solid phase carbon was detected in the depth range of 30 to 60 m (Fig. 4e). Note, though, that calcite was not identified in XRD spectra for samples taken from 27.7 and 74.7 m (Table 5). However, the detection limit for this method is approximately 0.5% by weight calcite, or approximately 10,000 times greater than the potential amount of calcite (0.2 to 2 μg/g) in this depth range if all of the inorganic carbon measured (0.02 to 0.2 ug/g; Fig. 4e) is incorporated in calcite. The dissolution of approximately 40 μg/g calcite, 200 to 20 times the amount possibly present now, would have been necessary to produce the peak dissolved Ca levels observed (Fig. 3k) assuming a porosity of 30% and using a density of 2.7 g/cm^3 for calcite if the calcite were dissolved into stagnant water. However, ample evidence indicates that the groundwater is flowing (Harvey et al., 2002), so the calcium concentrations measured at one location likely represent Ca that entered the groundwater along path lines extending from the source of recharge.

Other sources of Ca (and Fe) to these pore waters may include biotite and hornblende, as enhanced dissolution of silicate minerals by organic ligands has been observed in other studies (Manley and Evans, 1986; Mast and Drever, 1987; Chin and Mills, 1991). For Fe at least, XRD observations may support these claims; based on octahedral site refinements and ratio intensities of [004]/[005] peaks, the micas observed were consistently Fe-poor, suggesting that their dissolution may have contributed to the overall aqueous Fe budget. Calcium

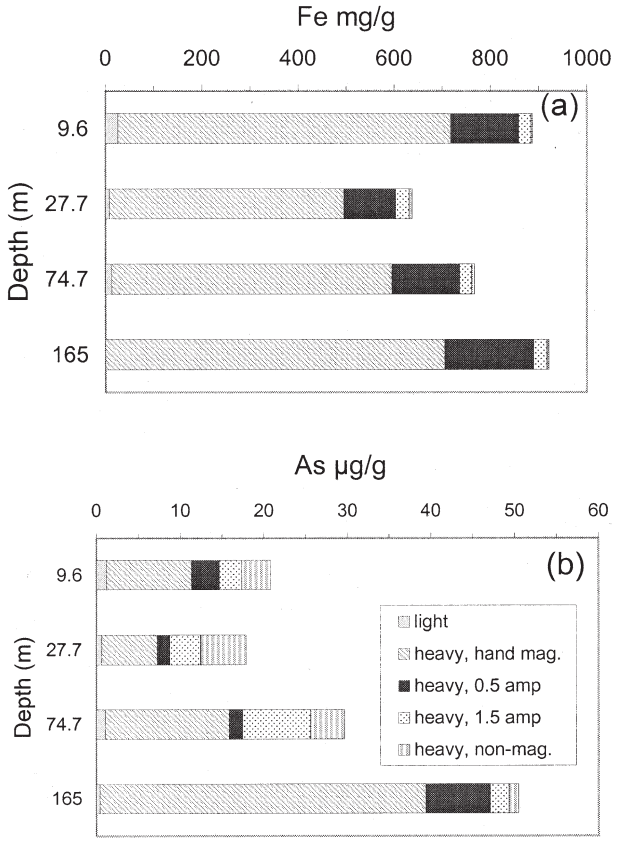

Fig. 8. Concentrations of (a) solid phase Fe (mg/g fraction), and (b) solid phase As (μg/g fraction) in the <2.85 g/cm^3 fraction and fractions >2.85 g/cm^3 separated by magnetic properties, including the hand-magnetic, 0.5 amp, and 1.5 amp, and nonmagnetic fractions; all for samples taken from depths of 9.6, 27.7, 74.7, and 165 m. The legend for both plots is shown in (b). Note that the hand-magnetic fraction consistently possesses the largest concentration of As by weight. See Table 3 for the relative abundances for the four depths analyzed and Table 4 for mineralogical characterization of fractions for the 27.7 m, 74.7 m, and 165 m depths.

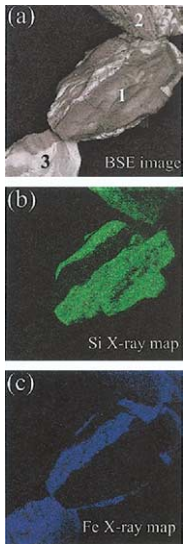

Fig. 9. SEM observations of Fe-rich coatings on mineral grains. (a) Backscatter image with a quartz (1) and feldspar (2) grain pictured from the 27.7 m hand magnetic fraction. Elemental composition is indicated with X-ray maps for (b) Si, and (c) Fe. Note the patches of Fe on these two grains. A magnetite grain (3) is also shown in the lower left corner of the backscatter image; magnetite makes up 98% of the hand magnetic fraction of the sample analyzed from this depth (see Table 4).

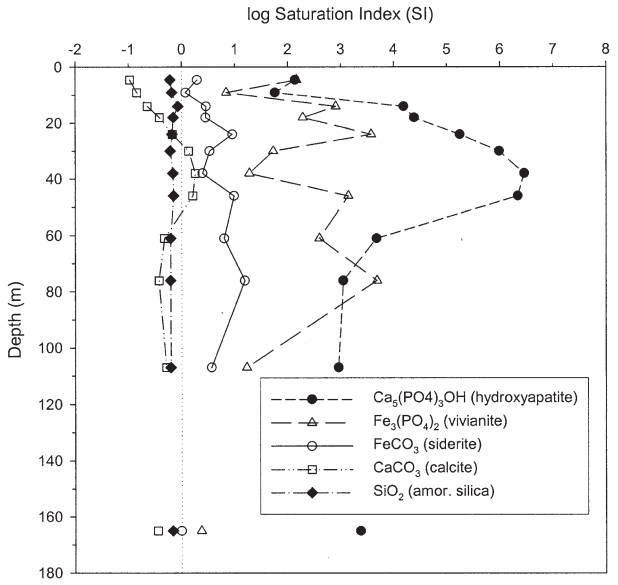

Fig. 10. Log saturation indices (SI) for hydroxyapatite [$Ca_5(PO_4)_3OH$], vivianite [$Fe_3(PO4)_2$], calcite [$CaCO_3$], siderite [$FeCO_3$], and amorphous silica (GL) [SiO_2] as a function of depth. A positive log SI indicates supersaturation with respect to the phase considered.

may also derive from dissolution of Ca-phosphate solids, which were observed as coatings on grains during SEM analyses of the density/magnetic separation fractions of these sediments (data not shown). The aqueous phase is supersaturated with respect to apatite [$Ca_5(PO_4)_3OH$] (Fig. 10).

Fe(II) generated in this geochemical system may not act conservatively, sorbing to solids or precipitating as Fe(II) or mixed valence solids, which may explain why dissolved As and Fe(II) profiles are not more correlated than observed here (compare Figs. 3a and 3e) or in Bangladesh aquifers elsewhere (Nickson et al., 2000; BGS & DPHE, 2001). Indeed, given the Fe/As ratios observed in these sediments, one would expect <1 μg/L levels of dissolved As in the pore water if congruent dissolution produced the mg/L quantities of dissolved Fe that are observed. The HCl-extractable pool of Fe, which comprised entirely Fe(II) for the several depths for which Fe was speciated, may include adsorbed Fe(II) or Fe(II) leached from solids such as siderite [$FeCO_3$] or vivianite [$Fe_3(PO_4)_2 \cdot 8H_2O$], both of which are supersaturated in the aqueous phase (Fig. 10) and are common products of biogenic Fe(III) oxyhydroxide reduction (Fredrickson et al., 1998; Zachara et al., 1998, Nickson et al., 2000). Other phases incorporating Fe(II) could include green rust and weakly crystalline magnetic phases (Fredrickson et al., 1998; Zachara et al., 1998; Banwart, 1999; Zachara et al., 2001). The relatively low levels of AVS measured in the sediments (Fig. 4c) indicate that little of the Fe(II) leached by the HCl extractant was incorporated in AVS (maximum of 0.1 $\pm$ 0.06%).

4.1.2. *Evidence for As adsorption limitation from extraction data*

Extraction data and X-ray microprobe analyses suggest that As is at least partly associated with Fe or Fe-rich phase(s) in these sediments. The substantial comapping of As and Fe fluorescence intensities observed in both upper (29.5 m) and lower aquifer (165 m) sediment samples (Figs. 7a,b), combined with the fact that As cumulatively leached by MG and PHOS extractants (interpreted as adsorbed As) does show some correlation with Fe cumulatively leached by the HCl, OX, and TiCEB extractants, may indicate that Fe or Fe-rich phase(s) dissolved by these extractants act as sorbents for the adsorbed As pool.

We constructed an isotherm to further explore associations between adsorbed and aqueous As, basing this exercise first on the assumption that the predominant sorbent comprises Fe liberated by the OX extractant, such as an amorphous Fe(III) oxyhydroxide phase, a mixed valence Fe phase such as magnetite (Dixit and Hering, 2003), and/or some Fe-rich weathering products associated with phyllosilicate minerals, as has been indicated by other studies (Foster et al., 2000; Breit et al., 2001). This model also assumes that the characteristics of the sorbent(s) do not vary with depth. The combined sum of MG- and PHOS-extractable As was first normalized by the sum of the OX-extractable Fe to determine the sorbed load of As per mole of OX-extractable Fe at each well depth; an average sorbed load was calculated for each depth from at least two different sediment samples. Average sorbed As loads were plotted for each well depth against their corresponding aqueous As concentrations (Fig. 11). For comparison, the similarly normalized adsorbed As loads determined using As leached by the pH 2 extractant are presented also (Fig. 11).

In each case, a Langmuir-like relation is apparent between the sorbed As load and aqueous As (Fig. 11). Langmuir isotherms generally indicate a saturation of sorbent surface sites (Morel and Hering, 1993). Depths with the highest aqueous As concentrations are characterized by a plateau at approximately

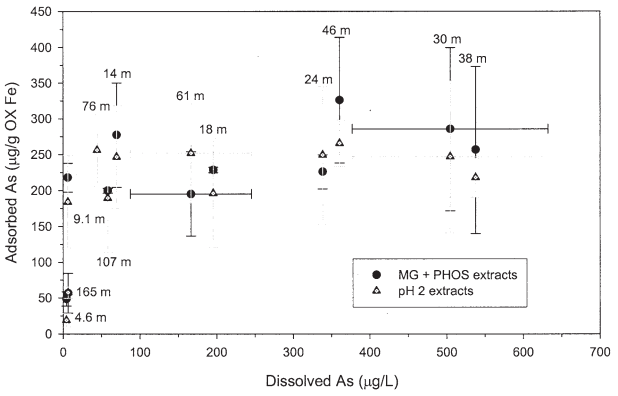

Fig. 11. The relation between adsorbed As loads (in μg As/g OX-extractable Fe) and aqueous As (in μg/L) for each well depth in the shallow and deeper aquifer. Adsorbed loads shown were determined by considering the sorbent as the sum of Fe liberated by the OX step and adsorbed As as that determined from either the pH 2 extracts (triangles) or from the sum of the MG and PHOS extracts (circles). The average $\pm$ one standard deviation (vertical error bars) are calculated from extraction data for at least two sample depths per well screen length. Aqueous As concentrations for the 30 m and 61 m depths are the average $\pm$ one standard deviation (horizontal error bars) of the levels measured in the three 30 m and two 61 m wells. Note the plateau in adsorbed As loads with increasing dissolved As concentrations in the aquifer, suggesting a saturation of sorbent surface sites available to As adsorption.

250 μg adsorbed As/g OX Fe, while levels of adsorbed As (in μg As/g OX-extractable Fe) fall below this plateau for well depths with low aqueous As concentrations, i.e., 4.6 and 165 m. It should be noted that even if the HCl-extractable pool of Fe, a quantity of Fe comparable to that leached by the OX step, and the relatively smaller pool of TiCEB-extractable Fe are considered cumulatively with the OX Fe in determining the As loads, a similar pattern between sorbed and aqueous As results, albeit with a lower plateau value (approximately 80 μg As/g [HCl + OX + TiCEB]-extractable Fe, data not shown). This relation between adsorbed loads and aqueous As suggests that one factor influencing the aqueous As depth profile at this site is a limited capacity to further sorb As at depths from 18 to 107 m, where aqueous As levels are greatest. Limited sorption results in part because As must compete with relatively higher levels of other oxyanions for available sorption sites, including bicarbonate (Fig. 3h), phosphate (Fig. 3j), and silicate (Fig. 3k), the latter quantified by measuring both aqueous silicon and molybdate-reactive silica concentrations, which are typically undifferentiable (Fig. 3k and Table 2).

The Langmuir-like relation between sorbed and dissolved As concentrations suggests some important characteristics of As mobility and transport in this aquifer. Because the sediment appears to have limited capacity to sorb additional As where dissolved As concentrations are above approximately 100 μg/L, As may be readily transported through regions where dissolved concentrations are high. Furthermore, As concentrations may be subject to more rapid change in these regions because any additional input of As, either by transport into the region or by mobilization from the local solid phase, will remain largely in the dissolved phase. These characteristics were confirmed in a large-scale injection-withdrawal experiment (Harvey et al., 2002) where high-As groundwater was displaced from approximately 32 m^3 of sediment by injection of low-As groundwater. The increase in As concentrations as this water was withdrawn was modeled with a rate-limited Langmuir isotherm coupled with an advective-dispersive model for transport from and to the well. They found that the data could not be reproduced with a linear isotherm (i.e., unlimited sites for sorption), but were closely reproduced by a Langmuir model very similar to that described here. Thus, this large-scale field experiment corroborates our finding that the sediment has little additional capacity to sorb As where concentrations are high.

4.1.3. Potential for ongoing influence of Fe(III) oxyhydroxides on As mobility

An important question to consider regarding the potential for ongoing As mobilization in the upper aquifer is whether Fe(III) oxyhydroxides remain a sorbent and coprecipitating phase for As in these sediments. If so, continued release of As through microbially mediated reductive dissolution of Fe(III) solids may be expected in the upper aquifer. Similarly, future elevations in dissolved As levels may result in the lower aquifer if reducing conditions intensify there, dissolving Fe(III) oxyhydroxides that are likely present, as suggested by the sediment coloring and relatively greater amounts of TiCEB-extractable Fe.

Harvey et al. (2002) also demonstrated in situ the potential for additional As release from the upper aquifer solids (at a depth of 105 m) after injecting groundwater amended with labile organic carbon (molasses) at concentrations similar to the total carbon concentration at the As peak in an effort to stimulate microbial respiration. Levels of As in water pumped from the injection depth rose within hours after injection of the amended groundwater, indicating the propensity of the aquifer solids for further As release (Harvey et al., 2002). The sensitivity of these aquifer solids to geochemical perturbations that release As to the pore water may be related to the fact that 10 to 20% of the total As measured in sediments from both the upper (and lower aquifer) is adsorbed (MG- and PHOS-extractable fractions, Table 3) and an additional 10 to 20% of As is coprecipitated in solids that are readily leachable with mild acids and reductants (HCl and OX extractants, respectively).

While the predominance of Fe(II) in the HCl-extractable pool of Fe in upper aquifer sediments suggests that geochemical conditions are not conducive to amorphous Fe(III) oxyhydroxide stability, amorphous Fe(III) oxyhydroxide could nevertheless exist, possibly associated with magnetite, quartz, feldspar and aluminosilicate grains as coatings, which were observed on the silicate minerals using SEM. The coexistence of Fe(II)and mixed valence solids such as magnetite, and possibly crystalline Fe(III) oxides, may indicate the absence of adequate reductant for complete reduction of the entire pool of available Fe(III).

We employed MINEQL^{TM} to explore how much of the OX-extractable Fe would have to comprise amorphous Fe(III) oxyhydroxide (HFO) to adequately predict the observed aqueous and adsorbed levels of key constituents (As, carbonate, phosphate, and silicate) in the upper aquifer. Here we used the 30 m well depth (a depth within the aqueous As peak) as an example. The objective was to compare the simulated quantity of HFO to measured levels of other sorbents, particularly magnetite, which makes up approximately 80% of the OX-extractable Fe at 27.7 m. Magnetite has recently been demonstrated to possess an intrinsic affinity for As(III) sorption similar to that of amorphous Fe(III) oxyhydroxide and goethite, although it has an approximately 10-fold lower sorption density than the former (Dixit and Hering, 2003).

Carbonate, phosphate, and silicate species were selected for analysis in the model because the aqueous levels of these constituents are substantial throughout the depth profile (Figs. 3h, j, and k) and there is evidence that each competes with As oxyanions for sorption sites on Fe(III) oxyhydroxides (Manning and Goldberg, 1996; Swedlund and Webster, 1999; Appelo et al., 2002). All simulations were run assuming total As comprised only As(III), as As(III) dominates the aqueous phase at 30 m (Fig. 3b) and initial simulations indicated As(III) species would overwhelmingly dominant the sorbed As pool also.

The modeled distribution of As between sorbed and aqueous pools was, as expected, highly sensitive to the amount of total Fe(III) present. Additionally, although observed aqueous As concentrations could be reproduced with the model by manipulating the amount of Fe(III) available for sorption, we found that aqueous silicate, phosphate, and Fe(II) species were consistently over-predicted.

Thus, additional simulations were conducted in which vivianite, siderite, and amorphous SiO_2 were allowed to precipitate

in addition to HFO. Note that the amount of phosphate in the pH 2 extractant, used to determine total phosphate in these simulations (Tables 1 and A1), may include some phosphate dissolved from solids such as vivianite in addition to adsorbed phosphate, especially if these solids have an amorphous nature. Similarly, silicon liberated by the pH 2 extractant (Tables 1 and A1) may comprise adsorbed silicate oxyanion and polymeric silica closely associated with surfaces. When we allowed precipitation of the additional phases, we were able to predict levels of dissolved As (460 μg/L), phosphate (3.8 mg/L), silicate (27.0 mg/L as Si), and Fe(II) (0.7 mg/L) reasonably close to average concentrations measured in the three 30 m wells (502 μg/L, 3.8 mg/L, 16.7 mg/L as Si, and 6.1 mg/L, respectively) using total Fe(III) equivalent to 2.5% (190 mg/L) of OX-extractable Fe.

Eliminating sorption of carbonate species to HFO in the model decreased dissolved As concentrations only slightly, to 375 μg/L. We found that silicate species were the dominant sorbate predicted in these simulations, with sorbed silicate concentrations approximately two, five, and ten times greater than sorbed carbonate species, phosphate and arsenite, respectively.

Although there are indications that surface complexation models may not be able to fully represent competitive adsorption effects (Ali and Dzombak, 1996), and natural sediments are often a complex mixture of multiple sorbents that may not possess the sorption properties of model laboratory-synthesized phases (Stollenwerk, 2003), the modeling results described above allow one to consider the relatively minor amount of amorphous Fe(III) oxyhydroxide, as a component of the labile pool of solid phase Fe (2.5% of OX-extractable Fe), that would be required to reproduce observed solute concentrations. This amount of an amorphous Fe(III) oxyhydroxide would be difficult to distinguish either wet-chemically or spectroscopically.

Given the considerably larger abundances of magnetite and aluminosilicate minerals, as well as possible Fe(II) solids whose presence is suggested by the HCl extracts, it may be that one or more of these constituents is the predominant sorbent for As in these sediments. Additional research is needed to (1) further characterize Fe-bearing solid phases and the Fe-rich coatings observed on mineral grains in these sediments; and (2) to determine specifically which phase(s) As is adsorbed to and coprecipitated with to better explain As mobility in these aquifers.

5. CONCLUSIONS

At the field site in Munshiganj, aqueous As levels in the upper aquifer are as high as 640 μg/L and are strongly depth-dependent. This pattern is explained neither by total solid phase As levels (which approximate crustal averages), nor by the proportions of total solid phase As distributed among various extractant pools. Adsorbed As appears to be at capacity at depths where aqueous As is greatest (i.e., the depth range of 30 to 40 m in the upper aquifer), with this sorption capacity determined considering the most labile fractions of solid phase Fe. One implication of this observation is that additional As mobilized nearby or transported to these depths in the upper aquifer would likely remain in the aqueous phase, with limited potential for mitigation by sorption to the solid phase.

The correlation between As and Fe in extracted fractions, and microscale comapping of As and Fe in the sediments observed with X-ray microprobe analysis provide evidence that As is associated with, at least in part, Fe or Fe-rich phases in both aquifers. These phases may include ubiquitous Fe coatings observed, using SEM-EDS, on quartz, feldspars, and other grains within sediment matrices. These phases could include ferrous or mixed-valence Fe solids; Fe extracted by 1 N HCl was found to comprise entirely Fe(II) in a few selected depths in the upper aquifer, consistent with the suboxic to anoxic conditions measured, and magnetite was observed in density and magnetic separations.

A role for Fe(III) oxyhydroxides in the upper aquifer can not be ruled out, however, as related studies (Harvey et al., 2002) at this site have found the upper aquifer to be susceptible still to As release upon introduction of labile organic matter, which presumably stimulated microbial respiration and possibly further reductive dissolution of Fe(III) solids to which the released As was associated. Equilibrium geochemical modeling conducted in the present study indicates that only a very small fraction (as little as 2.5%) of the Fe leached by oxalic acid from the sediments collected near the peak aqueous As depth (30 m), if present as an amorphous Fe(III) oxyhydroxide, could explain observed levels of adsorbed and dissolved As and levels of competing oxyanions silicate, phosphate and carbonate species, of which silicate was predicted to occupy the most sites. Note, though, that magnetite is substantially larger component of the sediment at this depth (80% of Fe leached by oxalic acid), and could serve as the predominant sorbent.

In the lower aquifer (with aqueous As levels of 4 μg/L), Fe-bearing solids appear to comprise a greater proportion of oxidized, crystalline Fe(III) based on comparison of color and supported by extraction data. This suggests that Fe(III) oxyhydroxides may be better preserved in the lower aquifer and that sorption capacity may mitigate an influx of As into the aquifer. The lower aquifer does have similar reducing conditions, levels of relatively mobile solid phase As, and concentrations of phosphate and silicate as the upper aquifer, though, suggesting that reductive dissolution of possible Fe(III) oxyhydroxide sorbents and competitive adsorption should be considered for possible future effects on As mobility in this aquifer also .

Acknowledgments— We gratefully acknowledge the assistance of the Bangladesh Department of Public Health Engineering in locating a field site and arranging for a drill rig and crew to perform the core collection and monitoring well installation for this study. We also wish to thank Steve Sutton and Matt Newville at Argonne National Lab for performing the X-ray microprobe analyses. The manuscript benefited greatly from the suggestions and comments of Alexander van Geen and two other anonymous reviewers. This work was funded in part by the National Science Foundation, grant EAR-0001098, National Institute of Health grant P30ES02109, and the Alliance for Global Sustainability.

Associate editor: P. O'Day

REFERENCES

Ali M. A. and Dzombak D. A. (1996) Competitive sorption of simple organic acids and sulfate on goethite. *Environ. Sci. Technol.* **30,** 1061–1071.

Anawar H. M., Akai J., Mostofa K. M. G., Safiullah S., and Tareq S. M. (2002) Arsenic poisoning in groundwater: Health Risk and geochemical sources in Bangladesh. *Environ. Int.* **27,** 597–604.

Appelo C. A., Van Der Weiden M. J. J., Tournassat C., and Charlet L. (2002) Surface complexation of ferrous iron and carbonate on ferrihydrite and the mobilization of arsenic. *Environ. Sci. Technol.* **36,** 3096–3103.

Badruzzaman A. B. M., Ahmed M. F., Hossain M. D., Jalil M. A., and Ali M. A. (1998) Arsenic contamination in groundwater in northeastern Bangladesh. *J. Civil Eng., IEB* **26** (*2*), 129–140.

Banwart S. A. (1999) Reduction of iron(III) minerals by natural organic matter in groundwater. *Geochim. Cosmochim. Acta* **63,** 2919–2928.

Berg M., Tran H. C., Nguyen T. C., Pham H. V., Schertenleib R., and Giger W. (2001) Arsenic contamination of groundwater and drinking water in Vietnam: A human health threat. *Environ. Sci. Technol.* **35,** 2621–2626.

Bhattacharya P., Chatterjee D., and Jacks G. (1997) Occurrence of arsenic-contaminated groundwater in alluvial aquifers from delta plains, Eastern India: Options for safe drinking water supply. *Water Res. Develop.* **13,** 79–92.

Breit G., Foster A. L., Whitney J. W., Uddin N. Md., Yount J. C., Welch A. H., Alam M. Md., Islam S. Md., Sutton S., and Newville M. (2001) Variable arsenic residence in sediment from eastern Bangladesh: clues to understanding arsenic cycling in the Bengal delta. Abstract presented at International Conference on Arsenic in Drinking Water, hosted by Columbia University Superfund Basic Research Program, Columbia University, November, 2001.

BGS & DPHE (British Geological Survey and Department of Public Health Engineering) (2001) Arsenic contamination of groundwater in Bangladesh (eds. D. G. Kinniburgh and P. L. Smedley). BGS Technical Report WC/00/19. British Geological Survey, Keyworth, UK.

Canfield D. E. (1989) Reactive iron in marine sediments. *Geochim. Cosmochim. Acta* **53,** 619–632.

Canfield D. E. and Berner R. A. (1987) Dissolution and pyritization of magnetite in anoxic marine sediments. *Geochim. Cosmochim. Acta* **51,** 645–659.

Chadha D. K. and Ray S. (1999) *High Incidence of Arsenic in Groundwater in West Bengal*. Central Government Board, Ministry of Water Resources, India.

Chin P. F. and Mills G. L. (1991) Kinetics and mechanisms of kaolinite dissolution: Effects of organic ligands. *Chem. Geol.* **90,** 307–317.

Chowdhury T. R., Basu G. K., Mandal B. K., Biswas B. K., Samanta G., Chowdhury U. K., Chanda C. R., Lodh D., Roy S. L., Saha K. C., Roy S., Kabir S., Quamruzzaman Q., and Chakraborti D. (1999) Arsenic poisoning in the Ganges delta. *Nature* **401,** 545–546.

Chowdhury U. K., Biswas B. K., Chowdhury T. R, Samanta G., Mandal B. K., Basu G. K., Chanda C. R., Lodh D., Saha K. C., Mukherjee S. K., Roy S., Kabir S., Quamruzzaman Q., and Chakraborti D. (2000) Groundwater arsenic contamination in Bangladesh and West Bengal, India. *Environ. Health Persp.* **108,** 393–397.

Cornell R. M. and Schindler P. W. (1987) Photochemical dissolution of goethite in acid/oxalate solution. *Clays Clay Miner.* **35,** 347–352.

Cullen W. R. and Reimer K. J. (1989) Arsenic speciation in the environment. *Chem. Rev.* **89,** 713–764.

Dixit S. and Hering J. G. (2003) Comparison of arsenic(V) and arsenic(III) sorption onto iron oxide minerals: Implications for arsenic mobility. *Environ. Sci. Technol.* **37,** 4182–4189.

Edwards M., Patel S., McNeill L., Chen H., Frey M., Eaton A. D., Antweiler R. C., and Taylor H. E. (1998) Considerations in As analysis and speciation. *J. AWWA* **90,** 103–113.

Foster A. L., Breit G. N., Welch A. H., Whitney J. W., Yount J. C., Islam M. S., Alam M. M., Islam M. K., and Islam M. N. (2000) In-situ identification of arsenic species in soil and aquifer sediment from Ramrail, Brahmanbaria, Bangladesh (abstract H21.D-01). *Eos***81** (*48*).

Fredrickson J. K., Zachara J. M., Kennedy D. W., Dong H., Onstott T. C., Hinman N. W., and Li S. M. (1998) Biogenic iron mineralization accompanying the dissimilatory reduction of hydrous ferric oxide by a groundwater bacterium. *Geochim. Cosmochim. Acta* **62,** 3239–3257.

Gibbs M. M. (1979) A simple method for the rapid determination of iron in natural waters. *Water Res.* **13,** 295–297.

Gruebel K. A., Davis J. A., and Leckie J. O. (1988) The feasibility of using sequential extraction techniques for arsenic and selenium in soils and sediments. *Soil Sci. Soc. Am. J.* **52,** 390–397.

Harvey C. F., Swartz C. H., Badruzzaman A. B. M., Keon-Blute N., Yu W., Ali A., Jay J., Beckie R., Niedan V., Brabander D., Oates P. M., Ashfaque K. N., Islam S., Hemond H. F., and Ahmed M. F. (2002) Arsenic mobility and groundwater extraction in Bangladesh. *Science* **298,** 1602–1606.

Huerta-Diaz M. A. and Morse J. W. (1992) Pyritization of trace metals in anoxic marine sediments. *Geochim. Cosmochim. Acta* **56,** 2681–2702.

Jakobsen R. and Postma D. (1999) Redox zoning, rates of sulfate reduction and interactions with Fe-reduction and methanogenesis in a shallow sandy aquifer, Rømø, Denmark. *Geochim. Cosmochim. Acta* **63,** 137–151.

Karim M. M. (2000) Arsenic in groundwater and health problems in Bangladesh. *Water Res.* **34,** 304–310.

Keon N. E., Swartz C. H., Brabander D. J., Harvey C., and Hemond H. F. (2001) Validation of an arsenic sequential extraction method for evaluating mobility in sediments. *Environ. Sci. Technol.* **35,** 2778–2784.

Lovley D. R. and Phillips E. J. P. (1986) Availability of ferric iron for microbial reduction in bottom sediments of the freshwater tidal Potomac River. *Appl. Environ. Microbiol.* **52** (*4*), 751–757.

Manley E. P. and Evans L. J. (1986) Dissolution of feldspars by low-molecular-weight aliphatic and aromatic acids. *Soil Sci.* **141,** 106–112.

Manning B. A. and Goldberg S. (1996) Modeling competitive adsorption of arsenate with phosphate and molybdate on oxide minerals. *Soil Sci. Soc. Am. J.* **60,** 121–131.

Mast M. A. and Drever J. I. (1987) The effect of oxalate on the dissolution rates of oligoclase and tremolite. *Geochim. Cosmochim Acta* **51,** 2559–2568.

Mazumder G. D. N., Haque R., Ghosh N., De B. K., Santra A., Chakraborti D., and Smith. A. H. (1998) Arsenic levels in drinking water and the prevalence of skin lesions in West Bengal, India. *Int. J. Epidemiol.* **27,** 871–877.

McArthur J. M., Ravenscroft P., Safiullah S., and Thirlwall M. F. (2001) Arsenic in groundwater: Testing pollution mechanisms for sedimentary aquifers in Bangladesh. *Water Resour. Res.* **37,** 109–117.

Morel F. M. M. and Hering J. G. (1993) *Principles and Applications of Aquatic Chemistry*. Wiley.

Nickson R., McArthur J., Burgess W., Ahmed K. M., Ravenscroft P., and Rahman M. (1998) Arsenic poisoning of Bangladesh groundwater. *Nature* **395,** 338.

Nickson R. T., McArthur J. M., Ravenscroft P., Burgess W. G., and Ahmed K. M. (2000) Mechanism of arsenic release to groundwater, Bangladesh and West Bengal. *Appl. Geochem.* **15,** 403–413.

Ostergren J. D., Brown G. E.Jr., Parks G. A., and Tingle T. N. (1999) Quantitative speciation of lead in selected mine tailings from Leadville, CO. *Environ. Sci. Technol.* **33,** 1627–1636.

Panias D., Taxiarchou M., Paspaliaris I., and Kontopoulos A. (1996) Mechanisms of dissolution of iron oxides in aqueous oxalic acid solutions. *Hydrometallurgy* **42,** 257–265.

Rogers C. E., Brabander D. J., Barbour M. T., and Hemond H. F. (2002) Use of physical, chemical and biological indices to assess impacts of contaminants and physical habitat alteration in urban streams. *Environ. Toxicol. Chem.* **21,** 1156–1167.

Ryan J. N. and Gschwend P. M. (1991) Extraction of iron oxides from sediments using reductive dissolution by titanium(III). *Clays Clay Miner.* **39,** 509–518.

Shimada N. (1996) Geochemical conditions enhancing the solubilization of arsenic into groundwater in Japan. *Appl. Organomet. Chem.* **10,** 667–674.

Smedley P. L. and Kinniburgh D. G. (2002) A review of the source, behaviour, and distribution of arsenic in natural waters. *Appl. Geochem.* **17,** 517–568.

Standard Methods for the Examination of Water and Wastewater (1992) Am. Pub. Health. Assoc., Am. Wat. Works. Assoc., Water Environ. Fed.

Stollenwerk K. G. (2003) Geochemical processes controlling transport of arsenic in groundwater: A review of adsorption. In *Arsenic in Ground Water: Geochemistry and Occurrence* (eds. A. H. Welch and K. G. Stollenwerk), pp. 67–100. Kluwer.

Swedlund P. J. and Webster J. G. (1999) Adsorption and polymerization of silicic acid on ferrihydrite and its effect on arsenic adsorption. *Water Res.* **33,** 3413–3422.

van Geen A., Zheng Y., Versteeg R., Stute M., Horneman A., Dhar R., Steckler M., Gelman A., Small C., Ahsan H., Graziano J. H., Hussain I., and Ahmed K. M. (2003a) Spatial variability of arsenic in 6000 tube wells in a 25 km^2 area of Bangladesh. *Water Resour. Res.* **39,** 1140., doi:10.1029/2002WR001617.

van Geen A., Ahmed K. M., Seddique A. A., and Shamsudduha M. (2003b) Community wells to mitigate the arsenic crisis in Bangladesh. *Bull. World Health Organ.* **81,** 632–638.

Welch A. H., Westjohn D. B., Helsel D. R., and Wanty R. B. (2000) Arsenic in ground water of the United States: Occurrence and geochemistry. *Ground Water* **38,** 589–604.

Yu W., Harvey C. M., and Harvey C. F. (2003) Arsenic in groundwater in Bangladesh: A geostatistical and epidemiological framework for evaluating health effects and potential remedies. *Water Resour. Res.* **39,** 1146.

Zachara J. M., Fredrickson J. K., Li S. M., Kennedy D. W., Smith S. C., and Gassman P. L. (1998) Bacterial reduction of crystalline Fe(III) oxides in single phase suspensions and subsurface materials. *Am. Mineral.* **83,** 1426–1443.

Zachara J. M., Fredrickson J. K., Smith S. C., and Gassman P. L. (2001) Solubilization of Fe(III) oxide-bound trace metals by a dissimilatory Fe(III) reducing bacterium. *Geochim. Cosmochim. Acta* **65,** 75–93.

Table A1. pH 2 extraction data for phosphate, silicon, and As.

Depth		Phosphate	Silicon	As
(m)	(ft)	(μg/g)	(μg/g)	(ng/g)
2.1	7	nm[a]	nm	nm
3.4	11	153	166	175
4.6	15	414	120	129
7.6	25	263	217	765
10.1	33	265	116	250
12.5	41	229	202	387
13.7	45	771	120	427
16.2	51	296	93.3	203
17.4	57	243	91.0	134
18.6	61	314	157	207
23.5	77	439	181	218
24.7	81	214	188	210
27.1	89	285	132	188
27.7	91	238	124	207
29.5	97	113	132	149
30.8	101	246	278	892
32.0	105	318	167	270
36.9	121	318	129	185
38.1	125	528	77.4	164
43.6	143	163	240	195
46.0	151	410	115	159
58.8	193	433	70.0	133
61.3	201	391	109	265
73.5	241	306	174	160
75.0	246	318	259	218
76.5	251	57.3	277	312
91.7	301	nm	nm	nm
104	341	208	188	146
107	351	356	157	123
122	401	nm	nm	nm
158	520	27.6	17.9	21.3
162	530	35.3	23.9	20.2
165	540	66.2	25.8	18.1

[a] Not measured